THE UNIVERSITY of EDINBURGH

Edinburgh Research Explorer

Strong intercorrelations among global graph-theoretic indices of structural connectivity in the human brain

Citation for published version:
Madole, JW, Buchanan, CR, Rhemtulla, M, Ritchie, SJ, Bastin, ME, Deary, IJ, Cox, SR & Tucker-Drob, EM 2023, 'Strong intercorrelations among global graph-theoretic indices of structural connectivity in the human brain', *NeuroImage*, vol. 275, 120160. https://doi.org/10.1016/j.neuroimage.2023.120160

Digital Object Identifier (DOI):
10.1016/j.neuroimage.2023.120160

Link:
Link to publication record in Edinburgh Research Explorer

Document Version:
Peer reviewed version

Published In:
NeuroImage

General rights
Copyright for the publications made accessible via the Edinburgh Research Explorer is retained by the author(s) and / or other copyright owners and it is a condition of accessing these publications that users recognise and abide by the legal requirements associated with these rights.

Take down policy
The University of Edinburgh has made every reasonable effort to ensure that Edinburgh Research Explorer content complies with UK legislation. If you believe that the public display of this file breaches copyright please contact openaccess@ed.ac.uk providing details, and we will remove access to the work immediately and investigate your claim.

OPEN ACCESS

Download date: 30. Jul. 2023

Strong intercorrelations among global graph-theoretic indices of structural connectivity in the human brain

James W. Madole[1,2*], Colin R. Buchanan[3,4], Mijke Rhemtulla[5], Stuart J. Ritchie[6], Mark E. Bastin[3,4,7], Ian J. Deary[3], Simon R. Cox[3,4], Elliot M. Tucker-Drob[1,8]

[1]Department of Psychology, University of Texas at Austin, Austin, TX

[2] VA Puget Sound Health Care System, Seattle Division, Seattle, WA

[3]Lothian Birth Cohorts, Department of Psychology, University of Edinburgh, Edinburgh, UK

[4]Scottish Imaging Network, A Platform for Scientific Excellence (SINAPSE) Collaboration, Edinburgh, UK

[5]Department of Psychology, University of California, Davis, Davis, CA

[6]Social, Genetic and Developmental Psychiatry Centre, King's College London, London, UK

[7]Centre for Clinical Brain Sciences, University of Edinburgh, Edinburgh, UK

[8]Population Research Center and Center on Aging and Population Sciences, University of Texas at Austin, Austin, TX

* Corresponding author

Correspondence to:

James W. Madole, M.A., Department of Psychology, The University of Texas at Austin, 108 E. Dean Keeton Street, Stop A8000, Austin, TX 78712, USA. E-mail: jmadole@utexas.edu

Running Head: GRAPH THEORY CORRELATIONS

Keywords: network neuroscience; connectomics; diffusion MRI; structural MRI; graph theory

Abstract

Graph-theoretic metrics derived from neuroimaging data have been heralded as powerful tools for uncovering neural mechanisms of psychological traits, psychiatric disorders, and neurodegenerative diseases. In $N = 8{,}185$ human structural connectomes from UK Biobank, we examined the extent to which 11 commonly-used global graph-theoretic metrics index distinct versus overlapping information with respect to interindividual differences in brain organization. Using unthresholded, FA-weighted networks we found that all metrics other than Participation Coefficient were highly intercorrelated, both with each other (mean $|r| = 0.788$) and with a topologically-naïve summary index of brain structure (mean edge weight; mean $|r| = 0.873$). In a series of sensitivity analyses, we found that overlap between metrics is influenced by the sparseness of the network and the magnitude of variation in edge weights. Simulation analyses representing a range of population network structures indicated that individual differences in global graph metrics may be intrinsically difficult to separate from mean edge weight. In particular, Closeness, Characteristic Path Length, Global Efficiency, Clustering Coefficient, and Small Worldness were nearly perfectly collinear with one another (mean $|r| = 0.939$) and with mean edge weight (mean $|r| = 0.952$) across all observed and simulated conditions. Global graph-theoretic measures are valuable for their ability to distill a high-dimensional system of neural connections into summary indices of brain organization, but they may be of more limited utility when the goal is to index separable components of interindividual variation in *specific* properties of the human structural connectome.

1. Introduction

Over the past decade, *network neuroscience* has emerged as the premier conceptual and methodological toolkit for interrogating the organizational properties of the human brain (Farahani, Karwowski, & Lighthall, 2019; Bassett & Sporns, 2017). Network models leverage formal mathematical principles derived from graph theory to represent systems of physical and functional connections within the brain (see Sporns, 2013 for review). In particular, human brain structural connectivity is commonly modelled as a network, or *structural connectome,* composed of discrete regions of grey matter (*nodes*) that are connected by white matter fibers (*edges*). By concomitantly accounting for thousands or more complex interactions from across distributed brain regions, network approaches are viewed as offering more granular and more specific insights into the neural foundations of human behavior and disease than approaches that restrict analyses to isolated brain areas (e.g., region-of-interest analyses) (Tompson, Falk, Vettel, & Bassett, 2018). The promise is that "[b]rain network organization" will reveal the "[neural] fingerprint[s] of specific disorder[s]." (van Montfort et al., 2019, pp. 1).

Graph-theoretic metrics are a popular method for capturing organizational information from brain networks (Sporns, 2013). Graph-theory is the mathematical study of graphs (or networks), which define pairwise relationships between objects, for example connectivity between brain regions. Commonly, indices that are defined at the level of individual network elements (i.e., *node-level* metrics) are averaged over the entire graph to provide a *global* reflection of how that network, writ large, instantiates a particular topological property (van Wijk, Stam, & Daffertshofer, 2010). For instance, average Degree has been used to measure "the extent to which the graph is connected," whereas average Betweenness "provides a measure of the 'hubness' of a network." (Wang, Zuo, & He, 2010, pp. 2; Haneef, Levin, & Chian, 2015, pp. 286).

The resultant metrics are considered especially valuable in neuroscience for two reasons: (1) they distill highly complex patterns of thousands of brain connections into what are thought to be meaningful low-dimensional summaries of a network's topology, and (2) their derived metrics are presumed to reflect distinct capacities of a neurological system (e.g., *integration*, *segregation*, *centrality*; see Rubinov & Sporns, 2010 for review) (see **Table 1** for overview of commonly-used metrics). As such, interindividual variability in these metrics is commonly interpreted as providing some insights into the neural mechanisms of individual differences in psychological traits (e.g., Baum et al., 2017; Kim et al., 2016), psychiatric disorders (e.g., Zhou et al., 2021; Yao et al., 2019), and neurodegenerative diseases (e.g., Berlot, Metzler-Baddeley, Ikram, Jones, & O'Sullivan, 2016; Pereira et al., 2015). When an association is observed between a network metric and an outcome such as cognitive function, the temptation is to make inferences that are specific to that pairing. For example, Li et al. (2009) inferred from such an observation that "the efficiency of brain structural organization," rather than some other organizational property or process, demarcates "an important biological basis for higher intelligence...[and] may provide new clues for understanding the mechanism of intelligence." (pp. 11). However, an empirical basis upon which to infer that such associations are, in fact, identifying a special meaning for a specific and distinct property of the brain is needed.

Here, we examine the discriminant validity of a commonly-used set of global graph-theoretic metrics in one of the largest samples of human structural connectomes to date (N = 8,185). To corroborate claims that an association between a particular metric and an outcome actually represents the neurological "fingerprint" of that outcome, we must first know how that metric relates to a broad array of other graph-theoretic metrics and to topology-free information (e.g., the average connectivity of the system, divorced from its organization). In the ensuing analyses, we empirically tackle the "current challenge …to determine the families of network diagnostics that provide complementary but not necessarily independent information about functional and anatomical brain organization.” (Bassett & Lynall, 2013, pp. 941).

The current study aims to provide a comprehensive account of the intercorrelations between of global graph-theoretic indices derived from adult human brain structural connectomes. In 8,185 healthy individuals from UK Biobank (UKB), we constructed structural connectivity networks and investigated patterns of intercorrelations between indices presumed to measure network integration, segregation, and centrality in the whole brain. We investigated whether the patterns of correlations were susceptible to variation based on edge weighting or thresholding scheme. We examined whether these indices are uniquely predictive of an external criterion (age) relative, one of the best known and most consistent correlates of brain MRI measures (see Cox & Deary, 2022 for review), to simpler, aggregate MRI indices. We contextualized our results in a series of simulation analyses. This is amongst the largest and most comprehensive studies of the explanatory validity of topological indices from structural connectivity indices to date.

2. Material & Methods

2.1 Participants

UK Biobank (UKB) is a population-based epidemiology study involving the collection and analysis of demographic, psychosocial, and medical data in over 500,000 individuals from across Great Britain from 2006 to 2010 (Sudlow et al., 2015). A subset of around 100,000 participants were selected to undergo MRI approximately four years after initial assessment. MRI data collection is still in progress, but portions of the data have been made available. At the time of processing a total of 9,858 participants with compatible T1-weighted and diffusion tensor (dMRI) data were available for analysis. All participants were imaged on the same scanner at the UKB imaging center in Cheadle, Manchester, UK. Exclusion criteria are provided below. The current sample is composed of $N = 8{,}185$ generally healthy individuals (4,315 females) with complete MRI data, ranging in age from 44.64 – 78.17 years (mean = 61.9; SD = 7.45). Over 97% of the sample self-identified as White. Substantial variability was evident in education level (college or university degree = 42.13%; high school qualification or equivalent = 44.02%; other professional qualification = 5.06%; none = 6.94%) and average total household income before tax (less than €18K = 11.86%; €18-31K = 21.76%; €31-52K = 27.65%; €52-100K = 22.85%; greater than €100K = 5.27%). UKB received ethical approval from the Research Ethics Committee (reference 11/NW/0382). All participants provided informed consent to participate. The current study was conducted under UKB application number 10279.

2.2 Brain Image Acquisition and Processing

2.2.1 *MRI.* All UKB participants were scanned on the same 3T Siemens Skyra MRI scanner (see Miller et al., 2016 and Alfaro-Almagro et al., 2018 for details). T-1 weighted volumes were acquired in the sagittal plane using a 3D MP-RAGE sequence. This data was preprocessed and analyzed by the UKB brain imaging team using FSL tools (http://www.fmrib.ox.ac.uk/fsl). A detailed description of the preprocessing analytic pipeline is available at https://biobank.ctsu.ox.ac.uk/crystal/crystal/docs/brain_mri.pdf. Using the raw FoV-reduced T-1 weighted volumes provided by UKB, we conducted local processing to reconstruct and segment the cortical mantle with default parameters in FreeSurfer v5.3 (Fischl & Dale, 2000; http://surfer.nrm.mgh.harvard.edu/) per the Desikan-Killiany atlas (Desikan et al., 2006). Automated anatomical segmentation of subcortical structures – accumbens area, amygdala, caudate, hippocampus, pallidum, putamen, thalamus, ventral diencephalon, and brain stem – was achieved using the same default settings in FreeSurfer (Fischl, 2012). FreeSurfer outputs were manually inspected to exclude participants with substantial motion artifact or gross errors in skull stripping, tissue segmentation, or cortical parcellation. 842 participants were excluded due to incomplete FreeSurfer output or inspection failure.

2.2.2 *Tractography.* Acquisition procedures for dMRI data are publicly available from the UKB website (http://biobank.ctsu.ox.ac.uk/crystal/refer.cgi?id=2367) (see Miller et al., 2016 for further details). dMRI data were acquired using a spin-echo echo-planar imaging sequence (50 b = 1000 s/mm_2, 50 b = 2000 s/mm_2, and 10 b = 0 s/mm_2, yielding 100 separate diffusion-encoding directions). The field of view was 104 x 104 mm with imaging matrix 52 x 52 and 72 slices with slice thickness of 2 mm, producing 2 x 2 x 2 mm voxels. The UKB team applied correction for head motion and eddy currents and then used BEDPOSTx to process the dMRI data with within-voxel modeling of multi-fiber (up to three fibers per voxel) tract orientation structure. Upon acquiring the data from UKB, we used PROBTRACKx to perform probabilistic tractography with cross-fiber modeling (Behrens et al., 2003). Streamlines were seeded from each white matter voxel using 100 Markov Chain Monte Carlo iterations with a fixed step size of 0.5 mm between successive points. 831 participants were excluded due to missing dMRI data or processing failure.

2.2.3 *Connectome Construction*. Whole-brain structural connectomes were constructed based on an automated connectivity mapping pipeline (Buchanan et al., 2014; Buchanan et al., 2015). T1-weighted volumes were decomposed into 85 discrete cortical and subcortical regions (*nodes*) per the Desikan-Killiany atlas (Desikan et al., 2006). Anatomical connections between nodes (*edges*; k = 3,570 possible edges) were estimated using six weighting schemes, reflecting different sources of information from dMRI thought to correspond with different properties of white matter. A whole-brain structural connectome, comprised of the 85 nodes and the 3,570 potential white matter edges, was therefore estimated six times for each participant in UKB. In a subset of n = 1500 randomly-selected participants, we used an alternative parcellation scheme that produces 375 cortical and subcortical nodes (Glasser et al. 2016). The k = 70,125 potential edges for this scheme were weighted using *fractional anisotropy* (see below for details).

2.2.4 *Weighting Schemes.* Networks were constructed by identifying edges between all pairs of nodes. Streamlines were tracked from seed locations to the first node encountered and recorded in an 85 x 85 connectivity matrix. Normalized *streamline count* (SC) – the count of all of the streamlines identified between nodes i and j divided by the highest observed streamline count value across all participants – served as a weighting scheme. Network metrics calculated using SC did not meaningfully differ before and after normalization (mean r between network metrics calculated with absolute SC and normalized SC > 0.99). Two further weightings were estimated from water diffusion parameters: *fractional anisotropy* (FA), a measure thought to reflect the degree of anisotropic water molecule diffusion; and *mean diffusivity* (MD), a measure thought to reflect the magnitude of the diffusion. Three weightings were estimated from neurite orientation dispersion and density imaging (NODDI; Zhang et al., 2012) parameters: *intra-cellular volume fraction* (ICVF), a measure thought to reflect neurite density; *isotropic volume fraction* (ISOVF), a measure thought to reflect extra-cellular water diffusion; and *orientation dispersion* (OD), a measure thought to reflect angular variation or fanning in neurite orientation. For each weighting scheme, individual edges were computed by estimating the mean value of the diffusion parameter in voxels identified along all interconnecting streamlines between nodes *i* and *j*. As is standard in the analysis of structural connectomes, all edges were considered undirected, resulting in a symmetric matrix. Diagonal elements – connections between a node and itself – were discarded for all matrices. Edge weights for all weighting schemes ranged from 0-1. We focus our primary analyses on FA-weighted connectomes, the most widely-used of these weighting schemes (Robinson et al., 2010; Verstraete et al., 2011). Additionally, we ran sensitivity analyses using binarized versions of FA-weighted matrices, wherein all present edges were coded as 1 and all absent edges were retained as 0.

2.2.5 *Thresholding Schemes.* Analyses were conducted with each weighting scheme using unthresholded networks (i.e., networks in which all estimated edges are retained). To examine the sensitivity of our results to potential thresholding effects, we applied both proportional and consistency-based thresholding in FA-weighted networks only. Thresholding schemes remove potentially false positive edges in favor of sparser and more anatomically-accurate representation of the brain. Proportional thresholding was applied by retaining only those edges that were estimated as non-zero in more than two-thirds of the sample. Consistency-based thresholding was applied by removing edges that exhibited evidence of inflated variability across participants and edges that were implausibly strong for their length, potentially indicating the presence of spurious edges in subsets of participants (Roberts et al., 2017; Buchanan et al., 2020). This thresholding level was set to retain 30% of connections.

2.3 Network Metrics

Commonly-used graph theoretic metrics were estimated using the *igraph* version 1.2.9 (Csardi & Nepusz, 2006) and *Network Toolbox* version 1.2.3 (Christensen, 2018) packages in *R*. To ensure proper estimation, metrics were estimated twice using either *igraph*, *Network Toolbox*, or *Brain Connectivity Toolbox* in Matlab and cross-validated. All metrics were confirmed to correlate at $r = 1.0$ across multiple estimation packages prior to running analyses. Network metrics were estimated for all UKB participants across each of the six weighting schemes and for both proportional and consistency-based thresholding schemes in FA-weighted networks only. Metrics were also estimated in unthresholded FA-weighted connectomes parcellated with the Glasser atlas. We prioritized estimating weighted metrics, but we report unweighted metrics when only unweighted versions exist or in situations in which weighted versions would be mathematically indistinguishable from other metrics of interest. This includes Degree (the number of adjacent edges connected to each node) and Density (the ratio of existing edges to possible edges). While there are multiple methods for estimating weighted versions of these metrics (Candeloro, Savini, & Conte, 2016; Darst, Reichman, Ronhovde, & Nussinov, 2013) both can become Strength if weighted (sum of edge weights connected to each node) and, if averaged across all nodes, can become perfectly collinear with mean edge weight. For these reasons, Strength and mean edge weight were excluded from the set of metrics estimated in binary networks.

Metrics are classified according to 5 categories: (a) *topologically-naïve*, summarizing the overall amount of connectivity in an individual's connectome that is not influenced by how the connections are organized; (b) *centrality*, reflecting the number or strength of connections to and from each node in the network, and thought to identify influential components of a system; (c) *integration*, reflecting the tendency for greater or stronger connections between different elements or clusters of brain regions, which is thought to reflect a network's ability to combine and process information from distributed brain regions; (d) *segregation*, reflecting the tendency for fewer or weaker connections between different elements or clusters of brain regions, which is thought to reflect the propensity for specialized processing to occur within interconnected groups of brain regions; and (e) *balance*, reflecting the propensity of a network to jointly achieve integration and segregation (Rubinov & Sporns, 2010; Joyce, Laurienti, Burdette, Hayasaka, 2010). To obtain a single value for each metric that could be compared across individuals, we computed the graph-level average of node-level metrics (i.e., the average value across all nodes), as has been done in previous literature (e.g., Degree (Wang, Zuo, & He, 2010); Strength (Hagmann et al., 2010); Betweenness (Haneef, Levin, & Chiang, 2015); Closeness (Rubinov, Sporns, van Leeuwen, & Breakspear, 2009); Participation Coefficient (Godwin, Barry, & Marois, 2015)). We focus on global versions of graph-theoretic metrics given that they have demonstrated greater reliability than local metrics (Andreotti et al., 2014) and that they hold the potential to summarize how different properties of the whole-brain connectome are structured. A detailed description of each network metric along with its mathematical derivation is provided in **Table 1**.

2.4 Data Preparation

Prior to running analyses, we examined distributions and descriptive statistics for each network metric. All network metrics displayed approximately normal distributions across each of the six weighting schemes. As the left frontal pole was found to be entirely disconnected in two participants, Characteristic Path Length was estimated as infinity in two participants. These participants were excluded from analyses with this metric.

Next, we estimated intercorrelations using Pearson correlation coefficients between each metric in conventional FA-weighted unthresholded structural brain networks. To examine whether graph-based network metrics relate to topologically-naïve summary indices, we correlated each metric with both mean edge weight and mean node weight. As the mathematical calculation of network metrics depends on properties of edges rather than nodes, we focus on mean edge weight as it provides a more direct comparison. To test whether network metrics were incrementally valid of one another and of topologically-naïve indices, we estimated each metric's correlation with age, before and after controlling for mean edge weight.

After thresholding, certain network metrics – Density, Degree, Betweenness, and Modularity – displayed skewed distributions, suggesting the presence of outliers. To test whether this skewness would bias correlations with other metrics, we transformed these variables to remove skewness. First, we winsorized each variable, by replacing outliers with mean(x) +/- 3.5*SD(x). For right skewed variables (Betweenness), we then took the square root of each value after subtracting the lowest value in the distribution and adding 0.1. For left skewed variables (Density and Degree), we reverse scored each variable before taking the square root in order to keep all values above 0, and then reverse scored once again after taking the square root. All variables displayed approximately normal distributions after these transformations. Correlations between originally-estimated variables and transformed variables were high across each metric (*r*'s > 0.865), suggesting that analyses of interindividual differences are likely to produce similar patterns of results regardless of whether the original or transformed variables are used. We therefore use original metrics in order to maintain the most direct comparability with metrics typically used in existing research.

2.5 Intercorrelations amongst graph-theoretic metrics across variable network conditions

To contextualize our findings in UKB connectomes, we conducted a series of secondary analyses examining the association between graph-theoretic metrics under variable network conditions. These analyses provide additional information for interpreting the magnitude of associations between graph-theoretic metrics, mean edge weight, and age in the observed UKB connectomes.

2.5.1 *Null network analyses*

We examined associations between the full set of graph-theoretic metrics, mean edge weight, and age in null networks constructed from unthresholded, FA-weighted UKB connectomes partialled by the Desikan-Killiany atlas. Following current recommendations for constructing null models (Váša & Mišić, 2022), we randomly reshuffled each of the k = 3,570 edges uniformly across participants, such that e.g., for each participant, $edge_1$ connecting $node_1$ and $node_2$ was replaced by $edge_{15}$. This approach preserves core architectural features of the network (e.g., degree; density distribution), while disrupting intrinsic network organization. Individual differences in graph-theoretic metrics and mean edge weight are retained because each randomly reshuffled edge weight still varies across participant.

2.5.2 Simulation analyses

To further examine how intercorrelations amongst global network metrics vary across a range of frequently observed network structures (i.e., *random*, *community-structured*, *small-world*), we conducted a series of toy simulation analyses. We provide further context for the analyses conducted in UKB connectomes by extending the scope of our investigation to include simulated network conditions under which we might expect global graph-theoretic metrics to be more or less separable from one another and from mean edge weight. Importantly, the toy simulations are comprised of 15 node networks and thus do not constitute a direct baseline reference to the UKB analyses.

We can represent a *population level* undirected connectome composed of *k* nodes as a symmetric $k \times k$ connectivity matrix C_{pop} taking the following form, with $k \times (k-1)/2$ nonredundant off-diagonal elements, *w* representing edge weights and subscripts indicating the pairs of nodes that they connect:

$$C_{pop} = \begin{bmatrix} & & & \\ w_{2,1} & & & \\ \vdots & & \ddots & \\ w_{k,1} & w_{k,2} & \cdots & w_{k,j} \end{bmatrix}$$

Nonzero values for a given weight $w_{k,j}$ represent the presence of the connection between pairs of nodes *i* and *j*, whereas values of 0 represent the absence of that connection. The specific nonzero value of *w* represents the strength of the connection. Depending on the configuration of *w*, we can specify population networks with different degrees of sparsity and different network types (e.g. random network, small-world network).

Given the population level connectome, C_{pop}, we can simulate individual connectomes (C_n) by drawing edge weights from a multivariate normal distribution:

$$vech[C_n] \sim \mathrm{N}\left(vech\left[C_{pop}\right], cov(w_{2,1} .. w_{k,j})\right)$$

where vech[C] represents the vectorized form of the connectivity matrix. This approach allows us to make various assumptions regarding the covariances among the edges, according to a $(k \times \frac{k-1}{2}) \times (k \times \frac{k-1}{2})$ covariance matrix taking the form:

$$cov(w_{2,1} \ldots w_{k,j}) = \Sigma = \begin{bmatrix} var(w_{2,1}) & & \\ \vdots & \ddots & \\ cov(w_{2,1}, w_{k,j}) & \ldots & var(w_{k,j}) \end{bmatrix}$$

The diagonal elements of Σ represent the variances of the weights, e.g. the extent to which fractional anisotropy varies across individuals. The off-diagonal elements of Σ may be set to 0 to represent a scenario in which the edges are uncorrelated, or they may be set to non-zero values to represent a scenario in which the edges covary with one another. Madole et al. (2020) reported a strong first principal component of edge weights within the FA-based structural connectome in the same data used here, indicating that a realistic scenario is one in which the off diagonal elements of Σ are positive and sizable.

Per these specifications, we conducted a series of toy simulations to examine how variation in network architecture influences associations between graph-theoretic metrics. We focused our simulations on three key attributes of network architecture: (1) *network type* (random, community-structured, or small-world network); (2) *network sparsity* (the proportion of non-zero edges); (3) *edge covariance* (the extent to which edge weights are related to one another). Network type and network sparsity were represented at the level of the population (C_{pop}). Edge covariance was specified by Σ. For each of the 18 population-level conditions, we simulated C_n = 1000 individual connectomes of 15 nodes, where individual differences in the set of C_{1000} networks were specified by Σ. A full description of each simulated condition is described below.

Within each of the C_{1000} simulated connectomes for each condition, we estimated the set of graph-theoretic metrics used in our primary analyses, as well as mean edge weight. We report the mean absolute correlation between graph-theoretic metrics with one another and with mean edge weight for each condition.

2.5.1 ***Random Networks.*** Random network architecture was generated by sampling population-level edge weights from a uniform distribution ranging from 0.30 to 0.80. Edge weights were sampled for each of the 105 non-redundant elements of the 15x15 matrix, representing a fully connected graph:

$$C_{pop} = \begin{bmatrix} w_{2,1} > 0 & & & \\ \vdots & w_{13,2} > 0 & \ddots & \\ w_{14,1} > 0 & w_{14,2} > 0 & & \\ w_{15,1} > 0 & w_{15,2} > 0 & \cdots & \end{bmatrix}$$

From this fully saturated population matrix, we generated C_{1000} individual connectomes according to two versions of Σ:

1. Where edges were moderately correlated with one another ($r = 0.5$):

$$cov(w_{2,1} \ldots w_{k,j}) = \Sigma = \begin{bmatrix} var(w_{2,1}) = .01 & & \\ \vdots & \ddots & \\ cov(w_{2,1}, w_{k,j}) = \ .005 & \ldots & var(w_{k,j}) = .01 \end{bmatrix}$$

2. Where edges were essentially uncorrelated with one another ($r = 0.05$):

$$cov(w_{2,1} \ldots w_{k,j}) = \Sigma = \begin{bmatrix} var(w_{2,1}) = .01 & & \\ \vdots & \ddots & \\ cov(w_{2,1}, w_{k,j}) = \ .00005 & \ldots & var(w_{k,j}) = .01 \end{bmatrix}$$

Variances were set at 0.01 (SD = 0.1) for each edge, meaning that, for any given edge, 95% of edge weights fell within a range of 0.4 units. Specifying variance at this level ensured that edges would meaningfully vary across simulated connectomes while not deviating drastically from the range of 0.3 to 0.8 established by C_{pop}. All edges were set as positive prior to running analyses by taking the absolute value of any negative edge.

In the UKB connectomes, the distribution of weights across participants for a given edge generally resembles a zero-inflated normal distribution in which streamlines are not present for some participants, with connection strengths distributed approximately normally for the participants for whom a given streamline exists. To achieve this in our simulations, between two and eight edges were randomly selected to be set to 0 in each individual connectome prior to thresholding. Because this results in the patterning of non-zero edges varying across individuals, it has the added benefit of producing variation in the unweighted network metrics (Density and Degree).

Thresholding masks were created by randomly selecting elements in the 15x15 matrix to be set to 0. Masks were created to impose sparsity at the level of 30%, 60%, and 90% nonzero connections. Masks were applied uniformly across each of the $k = 1000$ simulated networks, such that the same edges were removed from each network. In total, we tested associations between graph-theoretic metrics across six different conditions in random networks.

2.5.2 *Community-structured Networks.* Community-structured networks are defined as having sets of nodes that separate into distinct clusters, with numerous or strong edges within clusters and relatively fewer or weaker edges between clusters (Girvan & Newman, 2002). To simulate community-structured networks, we first assigned each of the 15 nodes to one of three clusters, ranging from 4-6 nodes. Edges for each of the 105 off-diagonal elements were then sampled from a uniform distribution, such that within-cluster edges were sampled from a distribution of "strong" connections ranging from 0.65 to 0.80 and between-cluster edges were sampled from a distribution of "weak" connections ranging from 0.10 to 0.30. The resulting population matrix was a fully connected graph. As with random networks, we created $k = 1000$ individual connectomes for each condition of edge covariance. Prior to thresholding, between one and five cross-cluster elements were randomly selected to be set to 0 in each individual connectome in order to impose variation in non-weighted network metrics.

Thresholding masks were created by randomly selecting cross-cluster elements to be set to 0. As in the random networks, masks were created to impose sparsity at the level of 30%, 60%, and 90% nonzero connections. Multiple metrics (e.g., Characteristic Path Length, Small Worldness) were undefined in 30% thresholded networks. As such, a thresholding mask was created to impose sparsity at the level of 40% nonzero connections, which returned estimates for all graph-theoretic metrics.

2.5.3 *Small-world Networks.* Small-world networks can be conceptualized as an intermediate between *lattice* networks (wherein nodes only connect to their k nearest neighbors) and *random* networks (wherein all edges are randomly sampled from the same probability distribution) (Bassett & Bullmore, 2017). A network is considered to have small-world properties if it has a sufficiently short average path length and high degree of clustering (Gibson & Vickers, 2016). In essence, small-world networks represent a lattice model in which (a) some neighboring nodes are not connected with one another and (b) some non-neighboring nodes are connected (i.e., high local and global efficiency) (Muldoon, Bridgeford, & Bassett, 2016). Networks are said to have small-world properties if the small-worldness metric s is greater than 1.0 ($s > 1.0$; Bassett & Bullmore, 2017).

To construct small-world networks, we first simulated a community-structured network (i.e., a network with three cluster of 4-6 nodes each, with strong within-cluster edges and weak between-cluster edges). Next, we randomly selected a proportion of weak between-cluster edges to be re-estimated as strong edges. We imposed thresholding on weak between-cluster edges only, such that 30%, 60%, or 90% of weak between-cluster edges were preserved. Said differently, thresholding schemes set 70%, 40%, or 10% of weak, between-cluster edges to 0, such that as the number of strong between-cluster edges increases, the number of weak between-cluster edges that gets set to 0 decreases because there are fewer weak connections to threshold. We then estimated Small Worldness using the equation displayed in Table 1. Small-world networks were achieved at the level of the population for all thresholding schemes when approximately half of the weak between-cluster edges were re-estimated as strong edges. As with other network types, we examined associations between graph-theoretic metrics across levels of thresholding and edge covariation.

***Table 1*. Overview of network metrics.**

Metric	Description	Type	Weighted	Level	Mathematical Derivation
Mean Edge Weight	Average of k = 3,570 potential edges, including zero-weighted edges.	Topologically-naïve	Weighted	Graph-level	$\overline{l^w} = \frac{l^w}{l}$
Mean Node Weight	Average of k = 85 node volumes.	Topologically-naïve	Weighted	Graph-level	$\overline{n^w} = \frac{\sum_{j\in N} n^w}{n}$
Density	Ratio of the number of present edges to the number of possible edges.	Centrality	Unweighted	Graph-level	$v = \frac{\sum a_{ij} = 1}{l}$
Degree	Number of edges connected to each node.	Centrality	Unweighted	Node-level	$k_i = \sum_{j\in N} a_{ij}$
Strength	Sum of the edge weights connected to each node.	Centrality	Weighted	Node-level	$k_i^w = \sum_{j\in N} w_{ij}$
Betweenness	Proportion of times a node lies on the shortest path between all other pairs of nodes.	Centrality	Weighted	Node-level	$b_i = \frac{1}{(n-1)(n-2)} \sum_{\substack{h,j\in N \\ h\neq j, h\neq i, j\neq i}} \frac{\rho_{hj}^{(i)}}{\rho_{hj}}$
Closeness	Inverse of the average length of the shortest paths to and from all other nodes in the network.	Centrality	Weighted	Node-level	$\left(L_i^w\right)^{-1} = \frac{n-1}{\sum_{j\in N, j\neq i} d_{ij}^w}$
Participation Coefficient	Strength of each node's intermodular connections. Communities empirically defined by Louvain clustering algorithm.	Centrality	Weighted	Node-level	$y_i^w = 1 - \sum_{m\in M} \left(\frac{k_i^w(m)}{k_i^w} \right)^2$
Characteristic Path Length	Average of the shortest path between each pair of nodes in the network.	Integration	Weighted	Graph-level	$L^w = \frac{1}{n} \sum_{i\in N} \frac{\sum_{j\in N, j\neq i} d_{ij}^w}{n-1}$
Global Efficiency	Average inverted shortest path length between each pair of nodes in the network.	Integration	Weighted	Graph-level	$E^w = \frac{1}{n} \sum_{i\in N} \frac{\sum_{j\in N, j\neq i} \left(d_{ij}^w\right)^{-1}}{n-1}$

Clustering Coefficient	Prevalence of clustered connectivity in the network (i.e., proportion of node's neighbors that are also neighbors of each other).	Segregation	Weighted	Graph-level	$C^w = \frac{1}{n}\sum_{i \in N} \frac{2t_i^w}{k_i\left(k_i - 1\right)}$
Modularity	Efficacy of a network's clustering arrangement. Clustering empirically defined by Louvain clustering algorithm.	Segregation	Weighted	Graph-level	$Q^w = \frac{1}{l^w}\sum_{i,j \in N}\left[w_{ij} - \frac{k_i^w k_j^w}{l^w}\right]\delta_{m_i m_j}$
Small Worldness	Extent to which network displays small world property: most nodes are not neighbors of one another, but neighbors are likely to be connected.	Balance	Weighted	Graph-level	$S^w = \frac{C^w / C^w_{rand}}{L^w / L^w_{rand}}$

Note. N = set of all nodes in the network; n = the number of nodes in the network; (i, j) is the edge between nodes i and j, where i and j are elements of N $(i, j \in N)$; a_{ij} is the connection status between i and j: $a_{ij} = 1$ when edge (i, j) exists, $a_{ij} = 0$ otherwise ($a_{ii} = 0$ for all i); L = set of all edges in the network; $l = \sum_{i,j \in N} a_{ij}$ = the number of edges in the network. The weights of edges (i, j) are represented as w_{ij}. All weights are normalized such that $0 \le w_{ij} \le 1$ for all i and j for all weighting schemes. $l^w = \sum_{i,j \in N} w_{ij}$ = the sum of all weights in the network. n^w = the weight of a given node, reflecting the total volume of each grey matter region as measured by T1-weighted imaging. ρ_{hj} = the number of shortest paths between h and j, and $\rho_{hj}^{(i)}$ = the number of shortest paths between h and j that pass through i. $d_{ij} = \sum_{a_{uv} \in g_{i \leftrightarrow j}} a_{uv}$ = the shortest path length (distance) between nodes i and j, where $g_{i \leftrightarrow j}$ is the shortest path between i and j. If no path exists between nodes i and j, $d_{ij} = \infty$, but was recoded as missing and those edges were excluded from analyses. M = set of nonoverlapping modules (or communities); m = a specific module; $\delta_{m_i m_j}$ = 1 if the module containing node i, m_i, = the module containing node j, m_j, and 0 otherwise.

$t_i^w = \frac{1}{2}\sum_{j,h \in N}\left(w_{ij} w_{ih} w_{jh}\right)^{\frac{1}{3}}$ = the weighted geometric mean of triangles acround node i. C^w_{rand} is the clustering coefficient of a random network with the same average degree as the observed network. Node-level metrics have subscript i on the left side of the equation to represent that the metric is calculated for each node. All node-level metrics were averaged across all nodes such that $\frac{1}{n}\sum_{i \in n}$ can be added to the beginning of the right side of the equation to represent its average. Edge weights for distance-based metrics (Betweenness, Closeness, Global Efficiency, and Characteristic Path Length) were inverted by taking the reciprocal of each edge weight (i.e., $1/w_{ij}$) prior to estimation using the *brainGraph* function in R (Watson, 2020). Louvain clustering algorithm, a multi-level modularity optimization algorithm for detecting communities within a network, was performed on a single network for each weighting scheme, where edges represented the median edge weight across all UKB participants. Metric descriptions and mathematical terminology and equations come from Rubinov & Sporns (2010). Additional information regarding network metrics comes from Christensen (2018).

3. Results

3.1 Unthresholded FA-weighted network metrics.

Correlations between the 11 different network metrics derived from unthresholded FA-weighted matrices were on average quite large (absolute range = 0.034 to 1.0; absolute interquartile range (IQR) = 0.502 to 0.936; mean $|r|$ = 0.645; **Fig. 1**). Approximately 44% (24 of 55 *r's*) of the pairwise associations between metrics were $|r| > 0.75$. Only 16.4% (9 of 55 *r*'s) of the pairwise associations were $|r| < 0.25$, each of which involved an association with Participation Coefficient, a measure of segregation based on the strength of each node's connections within its community. With the exception of Participation Coefficient, all metrics displayed strong correlations, on average, with one another (see **Table S1**), suggesting that these metrics are not strongly dissociable from one another. Magnitudes of intercorrelations between network metrics estimated from binary networks[1] were comparable to those from FA-weighted networks (absolute range = 0.054 to 1.0; absolute IQR = 0.121 to 0.978; mean $|r|$ = 0.642). Likewise, intercorrelations between metrics estimated from FA-weighted networks parcellated with the Glasser atlas (k = 375 nodes) in a random subset of n = 1500 UKB participants were comparable to those from networks parcellated with the Desikan-Killiany atlas (absolute range = 0.129 to 1.0; absolute IQR = 0.542 to 0.933; mean $|r|$ = 0.682).

To assess whether network metrics are distinct from summary indices of brain structure, we examined the relationship between each network metric and mean edge and node weight (**Fig. S1**). Correlations between mean edge weight and Strength were excluded from analyses as these are metrics that both aggregate across all non-zero edge weights and thus produce perfectly collinear estimates. Mirroring the pattern of intercorrelations amongst network metrics, mean edge weight displayed a weak correlation with Participation Coefficient ($|r|$ = 0.085), but was

[1] Under certain definitions, Strength is the weighted equivalent of Degree/Density and was therefore excluded from estimates of intercorrelations in unweighted networks to avoid redundancy.

strongly correlated with all other graph-based metrics (absolute range = 0.693 to 0.938; absolute interquartile range (IQR) = 0.842 to 0.932; mean $|r|$ = 0.873). Correlations between mean edge weight and Closeness, Characteristic Path Length, Global Efficiency, Clustering Coefficient, and Small Worldness were nearly perfectly collinear (|r’s| > 0.972). This same pattern was found in FA-weighted networks parcellated by the Glasser atlas ($|r|$ with Participation Coefficient = 0.318; mean $|r|$ with all other metrics excluding Strength = 0.867). This suggests that across unthresholded FA-weighted matrices of different sizes, structural brain indices derived from graph-theoretical principles and a topologically-naïve index of white matter microstructure provide very similar information with respect to interindividual differences in structural brain connectivity. Associations with mean node weight (cortical and subcortical regional volume) were small across all network metrics (absolute range = 0.010 to 0.136; absolute IQR = 0.053 to 0.106; mean $|r|$ = 0.078) consistent with previous work in this sample finding that edges and node volumes are generally unrelated to one another (Madole et al., 2021).

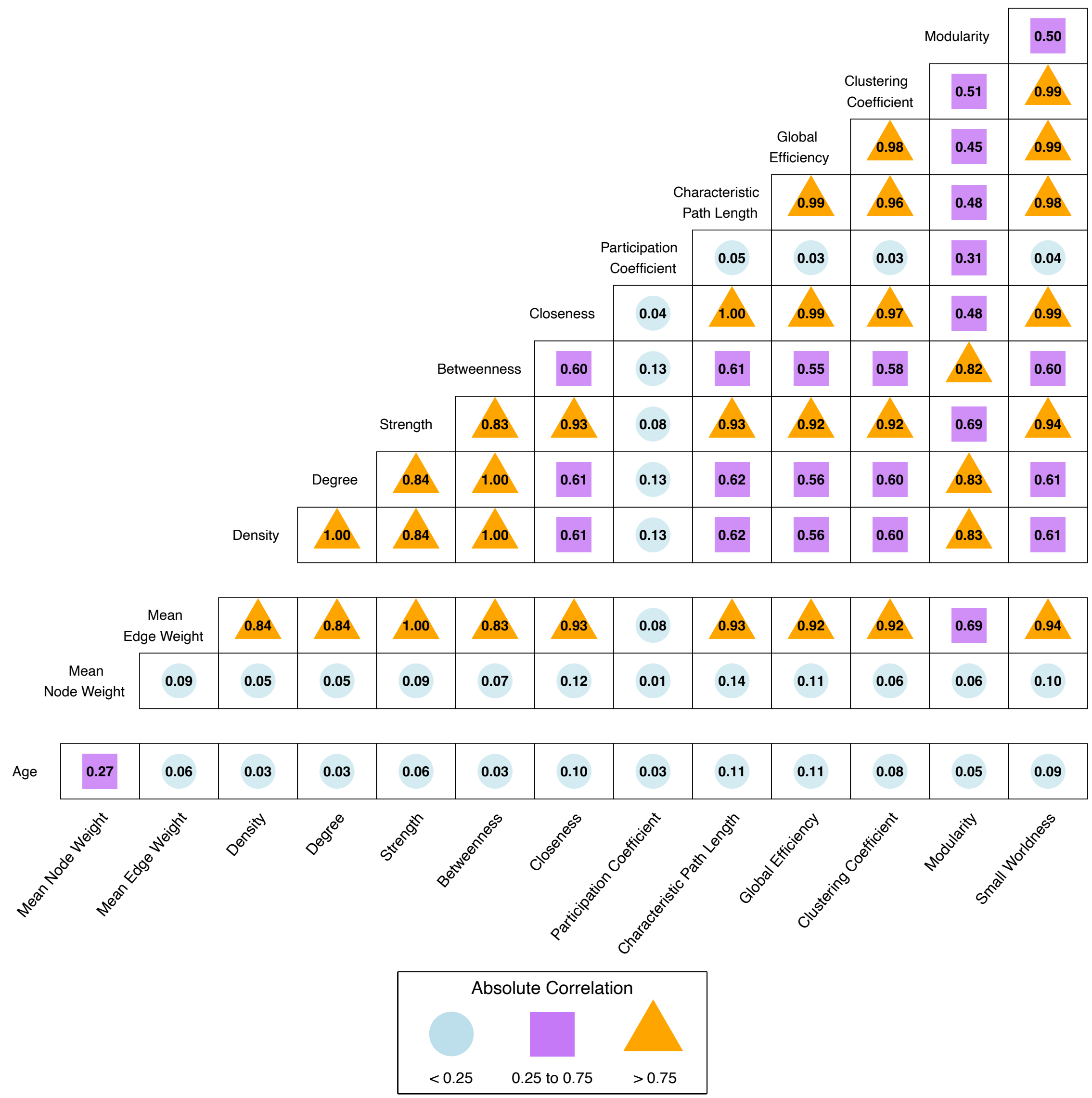

Figure 1. Correlations between ten global network metrics (unthresholded, FA-weighted), mean edge and node weight, and age. Cells display absolute correlations between each index for ease of interpretation.

3.2 Sensitivity analyses.

3.2.1 *Effects of thresholding on correlations between FA-weighted network metrics.*

To assess whether the large correlations between unthresholded FA-weighted network metrics were artifactually biased by the presence of spurious edges (Buchanan et al., 2020), we applied incrementally-stringent thresholding schemes to FA-weighted networks and re-estimated intercorrelations (see Method for details on thresholding schemes). Across both thresholding schemes, several metrics (Closeness, Characteristic Path Length, Global Efficiency, Clustering Coefficient, and Small Worldness) remained nearly perfectly collinear with one another (absolute r's > 0.976) and with mean edge weight (absolute r's > 0.941). Average correlations amongst all metrics, however, dropped considerably as a greater percentage of potentially spurious connections were removed (*proportional thresholding*: mean $|r| = 0.520$; *consistency-based thresholding*: mean $|r| = 0.379$; **Fig. S2**). The same trend was observed when examining intercorrelations between metrics in consistency-based thresholded binary networks (mean $|r| = 0.564$), though was not true in proportionally-thresholded binary networks (mean $|r| = 0.804$). Metrics from networks parcellated using the Glasser atlas remained strongly correlated across thresholding scheme (*proportional thresholding:* mean $|r| = 0.616$; *consistency-based thresholding*: mean $|r| = 0.630$).

Network metrics displayed marginally weaker associations with mean edge weight after applying proportional thresholding (mean $|r| = 0.698$), though displayed a more substantial average reduction after applying consistency-based thresholding (mean $|r| = 0.545$), suggesting that graph-based indices of network architecture and summary indices of white matter integrity may be at least somewhat more dissociable as networks become sparser. However, the same reduction in associations with mean edge weight was not observed in networks parcellated using the Glasser atlas (*proportional thresholding:* mean $|r| = 0.770$; *consistency-based thresholding*: mean $|r| = 0.779$).

To determine whether graph-theoretic metrics are incrementally predictive of an external criterion over and above mean edge weight, we examined zero-order correlations and standardized multiple regression coefficients between each graph-theoretic metric, mean edge weight, and age. We restrict our analyses to metrics derived from consistency-based thresholded networks, given previous work in this sample finding that associations between age and white-matter microstructure are most pronounced under this thresholding condition (Buchanan et al., 2020). All metrics other than Participation Coefficient showed small yet significant bivariate associations with age (r's = -0.051 to -0.187, p's < 0.0005; **Table 2**). In multiple regression analyses, associations with Closeness, Characteristic Path Length, Global Efficiency, Clustering Coefficient, and Small Worldness suffered from issues of multicollinearity with mean edge weight (i.e., highly inflated standard error relative to standard error of bivariate association; regression estimates inflated relative to bivariate association; sign changing from negative to positive across bivariate and multiple regression associations). Associations including Density, Degree, Participation Coefficient, and Modularity did not suffer from issues of multicollinearity, though Modularity was the only one of these metrics to be significantly predictive of age over and above mean edge weight ($b = -0.175$; $p < 0.0005$). To note, issues of multicollinearity varied slightly across thresholding schemes, but were in general more strongly pronounced under unthresholded and proportional thresholded conditions.

***Table 2*. Associations between global graph-theoretic metrics, mean edge weight, and age in consistency-based thresholded FA networks.**

Metric	Correlation with Age (SE)	Correlation with Mean Edge Weight (SE)	Beta1 (Age ~ Mean Edge Weight (controlling for graph metric in column 1)) (SE)	Beta2 (Age ~ Graph Metric (controlling for Mean Edge Weight)) (SE)
Mean Edge Weight	-0.178 (0.011)*	1.0 (0.000)	-0.178 (0.011)*	N/A
Density	-0.051 (0.011)*	0.197 (0.011)*	-0.174 (0.011)*	-0.017 (0.011)
Degree	-0.051 (0.011)*	0.197 (0.011)*	-0.174 (0.011)*	-0.017 (0.011)
Strength	-0.178 (0.011)*	1.0 (0.000)	-0.178 (0.011)*	N/A
Betweenness	-0.043 (0.011)*	-0.105 (0.011)*	-0.182 (0.054)*†	-0.062 (0.011)*
Closeness	-0.149 (0.011)*	0.978 (0.002)*	-0.182 (0.011)	0.004 (0.367)†
Participation Coefficient	-0.012 (0.011)	-0.019 (0.011)	-0.178 (0.011)*	-0.015 (0.011)
Characteristic Path Length	0.150 (0.011)*	-0.973 (0.003)*	-0.585 (0.046)*†	-0.419 (0.047)*†
Global Efficiency	-0.157 (0.011)*	0.991 (0.001)*	-1.060 (0.076)*†	0.901 (0.076)*†
Clustering Coefficient	-0.187 (0.011)*	0.992 (0.001)*	0.367 (0.087)*†	-0.573 (0.086)*†
Modularity	-0.178 (0.011)*	0.013 (0.011)	-0.175 (0.010)*	-0.175 (0.010)*
Small Worldness	-0.168 (0.011)*	0.986 (0.002)*	-0.426 (0.066)*†	0.237 (0.066)*†

Note. SE= standard error. * = *p*-value < 0.0005. † = issues of multicollinearity (inflated standard error relative to standard error of bivariate association; regression estimates inflated relative to bivariate association; sign changing from negative to positive across bivariate and multiple regression associations), estimates should be interpreted with caution.

3.2.2 ***Effects of dMRI weighting schemes on correlations between network metrics.***

To examine whether the pattern of intercorrelations observed amongst network metrics calculated from FA-weighted matrices was specific to the properties of that weighting scheme, we conducted the same set of analyses in five alternative dMRI weighting schemes thought to capture different white matter properties (ICVF = Intra-cellular volume fraction; ISOVF = Isotropic volume fraction; MD = Mean diffusivity; OD = Orientation dispersion; SC = Streamline count (normalized)) (see Method for details). Within weighting schemes, magnitudes of correlations between network metrics were on average modestly weaker than those estimated using FA (mean $|r\text{'s}|$ = 0.379 to 0.593; see **Table 3A**, **Figure S3**). Associations with mean edge weight were also marginally weaker than those estimated using FA, but were still strong (mean $|r\text{'s}|$ = 0.538 to 0.753; see **Table 3B**, **Figure S3**). To explore potential sources of discrepancy across weighting scheme, we examined the average correlation amongst network metrics and mean edge weight in relation to an estimate of variation between edge weights within each scheme (average coefficient of variation (CoV) across each participant), given previous research that has suggested that "variability of connection weights within systems...may be an important feature...of [the] connectome." (Jo, Faskowitz, Esfahlani, Sporns, & Betzel, 2021, pp. 8). We found that the average correlation amongst network metrics and the average correlation with mean edge weight were both strongly related to the degree of variation in edge weights (r's between mean $|r\text{'s}|$ amongst network metrics and with mean edge weight and average CoV < -0.64), such that associations between graph-theoretic metrics themselves and with non-network summary indices of brain structure are more independent in weighting schemes that impose a greater degree of variation in edge weights.

To determine whether the pattern of intercorrelations was stable amongst weighting schemes, we correlated the set of 55 correlations estimated within each weighting scheme with the set of correlations estimated in each other weighting scheme (k = 15 correlations between the set of correlations from each weighting scheme). Correlations estimated across weighting scheme were strongly related to one another (mean r = 0.813; range = 0.602 to 0.967), indicating that the relative magnitudes of collinearity amongst metrics is preserved across weighting scheme differences. **Figure 2** displays the average pairwise correlation between each metric across the six weighting schemes. Across weighting schemes, correlations with Participation Coefficient were small and highly stable (mean $|r|$ = 0.120; mean SD for each pairwise correlation with Participation Coefficient = 0.069). Similar to thresholding analyses, correlations between Closeness, Characteristic Path Length, Global Efficiency, and Small Worldness were, on average, strong and stable across weighting scheme (mean $|r|$ = 0.965; mean SD for each pairwise correlation = 0.052), with the exception of Clustering Coefficient which displayed somewhat smaller and more variable associations with this group of metrics across schemes (mean $|r|$ = 0.804; mean SD for each pairwise correlation = 0.297). These metrics also displayed some of the strongest and most stable associations with mean edge weight (mean $|r|$ = 0.872; mean SD for each pairwise correlation = 0.105). In other words, the metrics examined tended to be strongly related to overall white matter connectivity, irrespective of how this microstructure is measured.

Table 3. **Average absolute intercorrelation between network metrics and between network metrics and mean edge weight estimated within each weighting scheme using unthresholded networks.**

Weighting Scheme	**A. Average correlation amongst network metrics**		**B. Average correlation with mean edge weight**	
	SD	**IQR**	**SD**	**IQR**
FA	0.645		0.794	
	0.315	0.502 to 0.936	0.260	0.835 to 0.930
ICVF	0.593		0.753	
	0.324	0.399 to 0.952	0.261	0.701 to 0.942
ISOVF	0.398		0.595	
	0.376	0.071 to 0.859	0.351	0.237 to 0.875
MD	0.485		0.673	
	0.339	0.207 to 0.867	0.296	0.690 to 0.870
OD	0.542		0.717	
	0.320	0.225 to 0.850	0.197	0.715 to 0.828
SC	0.379		0.538	
	0.338	0.102 to 0.698	0.377	0.206 to 0.919

Note. FA= Fractional anisotropy; ICVF = Intra-cellular volume fraction; ISOVF = Isotropic volume fraction; MD = Mean diffusivity; OD = Orientation dispersion; SC = Streamline count (normalized); IQR = Interquartile range. Note that Strength is excluded from associations with mean edge weight because these are perfectly collinear estimates. Note that the association presented between FA and mean edge weight is lower than the one presented in the text due to the inclusion of Participation Coefficient.

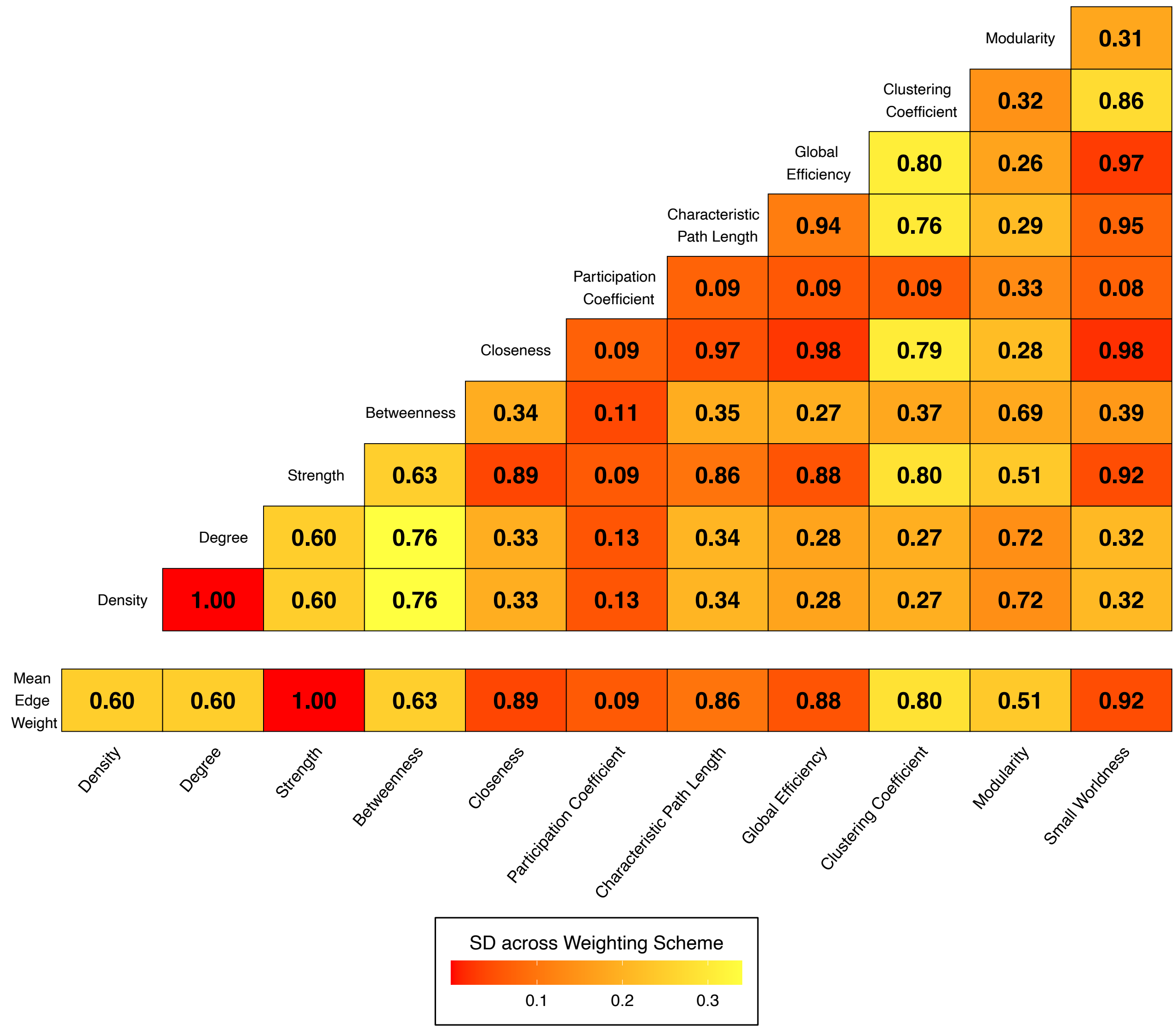

Figure 2. Average absolute correlation between each network metric and with mean edge weight across each of the six weighting schemes (FA, ICVF, ISOVF, MD, OD, SC). Color scale represents variation in associations across weighting scheme, such that red cells indicate pairwise associations that are stable across weighting scheme and yellow cells indicate pairwise associations that tend to vary across weighting scheme. Diagonal elements (i.e., the average correlation between a metric and itself across weighting schemes) were all estimated as 1 and are excluded here for ease of interpretation.

3.3 Intercorrelations amongst graph-theoretic metrics across null and simulated network conditions

3.3.1 *Null analyses*

To contextualize our findings in the UKB sample, we estimated absolute correlations amongst the 11 graph-theoretic metrics estimated in primary analyses and mean edge weight in a degree-preserving null network. Average absolute associations between each metric were comparable to those in the observed UKB connectomes (absolute range = 0.010 to 1.0; absolute IQR = 0.285 to 0.861; mean $|r|$ = 0.600). Likewise, average absolute associations with mean edge weight remained robust (mean $|r|$ = 0.836), largely driven by the nearly perfect collinearity between mean edge weight, Closeness, Characteristic Path Length, Clustering Coefficient, and Small Worldness ($|r$'s$| > 0.916$). Of interest, Global Efficiency showed somewhat greater differentiation from this set of metrics than it did other under network conditions (mean $|r|$ = 0.547).

3.3.2 *Simulation analyses*

We estimated absolute correlations amongst the 11 graph-theoretic metrics estimated in primary analyses and mean edge weight in a series of simulated networks (k = 1000 networks per condition; c = 18 conditions; see **Table 4**). Networks were comprised of 15 nodes and 105 potential edges. Networks varied by network type (i.e., random, community-structured, and small-world networks), the magnitude of covariation amongst the edge weights, and the proportion of non-zero connections (see Method for full description).

As with our observed data, we found that Closeness, Characteristic Path Length, Global Efficiency, Clustering Coefficient, and Small Worldness were nearly perfectly collinear with one another (mean r's = 0.785 to 0.990) and with mean edge weight (mean r's = 0.746 to 0.995) across all simulated conditions. Degree, Strength, Betweenness, Participation Coefficient, and

Modularity showed relatively greater discriminancy with one another and with mean edge weight, particularly in small-world networks (mean r's between metrics = 0.129 to 0.249; mean r's with mean edge weight = 0.102 to 0.395), making it possible that this subset of graph-theoretic metrics may capture some unique aspects of brain topology, independent of connection weight, under specific conditions.

Average correlations amongst graph-theoretic metrics varied across conditions, with mean correlations being highest in community-structured networks with strong covariation amongst edges (mean r's = 0.632 to 0.648) and lowest in small-world networks with weak covariation amongst edges (mean r's = 0.341 to 0.366). Metrics displayed strong average correlations with mean edge weight across all conditions (mean r's = 0.521 to 0.780), indicating that the large associations between graph-theoretic metrics and mean edge weight are not simply artifacts of network type, sparsity, or edge covariation. As with the UKB data, we found that sparser networks tended to yield marginally more discriminant metrics, and demonstrated that this may be particularly true in networks where the edges are uncorrelated. It is important to note that, whereas the magnitudes of association between graph-theoretic metrics and mean edge weight were relatively high across all conditions, they were somewhat lower relative to our empirical findings in UKB. This is notable given that the observed UKB connectomes have a high degree of small-worldness (mean s in unthresholded FA-networks = 1.28), but may be, at least in part, driven by the sizable correlations between edges in UKB (Madole et al., 2021).

***Table 4*. Simulation results: average absolute correlations between graph-theory metrics for FA-like networks.**

			All Metrics		**Group 1 Metrics**		**Group 2 Metrics**		**Group 1-2 Metrics**
Network Type	Threshold	Edges	rMetrics_Mean (SD)	rMEW_Mean (SD)	rMetrics_Mean (SD)	rMEW_Mean (SD)	rMetrics_Mean (SD)	rMEW_Mean (SD)	rMetrics_Mean (SD)
Random	90	Correlated	0.511 (0.409)	0.682 (0.409)	0.989 (0.010)	0.994 (0.005)	0.311 (0.293)	0.444 (0.374)	0.427 (0.341)
Random	60	Correlated	0.500 (0.408)	0.669 (0.413)	0.983 (0.012)	0.990 (0.006)	0.303 (0.291)	0.407 (0.385)	0.382 (0.348)
Random	30	Correlated	0.470 (0.359)	0.634 (0.380)	0.911 (0.071)	0.948 (0.057)	0.307 (0.234)	0.358 (0.316)	0.318 (0.273)
Random	90	Uncorrelated	0.468 (0.355)	0.650 (0.367)	0.980 (0.017)	0.980 (0.010)	0.263 (0.148)	0.319 (0.201)	0.265 (0.173)
Random	60	Uncorrelated	0.442 (0.353)	0.633 (0.366)	0.942 (0.054)	0.958 (0.018)	0.228 (0.172)	0.292 (0.219)	0.229 (0.162)
Random	30	Uncorrelated	0.492 (0.256)	0.641 (0.275)	0.785 (0.195)	0.869 (0.151)	0.402 (0.114)	0.401 (0.148)	0.322 (0.134)
Community-structured	90	Correlated	0.648 (0.444)	0.780 (0.399)	0.969 (0.030)	0.984 (0.023)	0.579 (0.472)	0.713 (0.459)	0.703 (0.412)
Community-structured	60	Correlated	0.642 (0.430)	0.769 (0.401)	0.966 (0.030)	0.979 (0.024)	0.561 (0.465)	0.696 (0.458)	0.693 (0.388)
Community-structured	40	Correlated	0.632 (0.363)	0.742 (0.353)	0.939 (0.048)	0.958 (0.044)	0.568 (0.336)	0.634 (0.374)	0.633 (0.337)
Community-structured	90	Uncorrelated	0.580 (0.370)	0.713 (0.338)	0.936 (0.050)	0.941 (0.038)	0.504 (0.336)	0.578 (0.329)	0.549 (0.324)
Community-structured	60	Uncorrelated	0.544 (0.343)	0.663 (0.314)	0.892 (0.098)	0.896 (0.055)	0.474 (0.297)	0.505 (0.272)	0.487 (0.290)
Community-structured	40	Uncorrelated	0.469 (0.310)	0.521 (0.288)	0.786 (0.215)	0.746 (0.117)	0.374 (0.246)	0.348 (0.205)	0.406 (0.259)
Small-world	90	Correlated	0.476 (0.431)	0.657 (0.438)	0.988 (0.010)	0.994 (0.010)	0.249 (0.305)	0.395 (0.401)	0.384 (0.356)
Small-world	60	Correlated	0.469 (0.404)	0.651 (0.414)	0.989 (0.010)	0.995 (0.010)	0.228 (0.246)	0.366 (0.315)	0.354 (0.283)
Small-world	30	Correlated	0.429 (0.396)	0.613 (0.427)	0.990 (0.010)	0.995 (0.010)	0.194 (0.169)	0.273 (0.223)	0.261 (0.202)
Small-world	90	Uncorrelated	0.363 (0.398)	0.564 (0.435)	0.945 (0.051)	0.967 (0.014)	0.150 (0.140)	0.179 (0.150)	0.142 (0.135)
Small-world	60	Uncorrelated	0.366 (0.395)	0.560 (0.438)	0.952 (0.046)	0.971 (0.011)	0.167 (0.140)	0.157 (0.100)	0.122 (0.091)
Small-world	30	Uncorrelated	0.341 (0.416)	0.535 (0.469)	0.962 (0.036)	0.977 (0.010)	0.129 (0.174)	0.102 (0.085)	0.081 (0.073)

Note. Group 1 metrics = Closeness, Characteristic Path Length, Global Efficiency, Clustering Coefficient, Small Worldness. Group 2 metrics = Degree, Strength, Betweenness, Participation Coefficient, Modularity. Density was excluded from Group 2 metrics due to perfect collinearity with Degree. Strength was removed from all estimates with mean edge weight due to mathematical equivalency and was removed from correlations between Group 1 & 2 metrics given the nearly perfect associations between Group 1 metrics and mean edge weight. Community-structured networks were thresholded at the level of 40% non-zero connections due to certain metrics being undefined at 30% thresholding. Thresholding for small-world networks applied only to weak, between-cluster connections and therefore preserved a greater number of non-zero connections than other network types.

4. Discussion

Graph-theoretic indices are a common tool for indexing various aspects of the topological organization of structural brain networks (Sporns, 2013). Particularly in light of recently highlighted challenges to estimating unbiased, reproducible estimates of brain-behavior associations from high-dimensional brain imaging data (Marek, 2022), global graph-theoretic metrics are especially appealing in their ability distill the organization of thousands of brain connections into low-dimensional summary indices. In a large sample of human structural connectomes from middle-aged and older adults in UK Biobank (UKB), we examined associations between commonly-used global graph-theoretic metrics with (a) one another, (b) topologically-naïve indices of brain structure, and (c) an external criterion (age). We found that across unthresholded FA-weighted networks of variable node sizes, all metrics other than Participation Coefficient were highly correlated, both with each other and with a topologically-naïve summary index of brain microstructure. Removing potentially spurious edges improved the dissociability of metrics in FA-weighted networks. However, even after this procedure, several commonly-used metrics (Clustering Coefficient, Closeness, Characteristic Path Length, Global Efficiency, Small Worldness) remained nearly perfectly collinear with one another and with mean edge weight across several observed and simulated conditions. Graph-theoretic metrics varied in their average associations with one another across alternative dMRI weighting schemes, such that schemes that imposed greater variation in edge weights yielded more discriminant metrics. Pairwise associations between metrics nevertheless tended to be consistent in magnitude across weighting scheme, even for other commonly-used weighting schemes such as streamline count.

Investigations of the interrelations amongst graph-theoretic metrics outside of a neuroscience framework have indicated that theoretically-distinct metrics at both a local and global level can be highly collinear (Kogotkova, Oehlers, Ermakova, & Fabian, 2018; Strang, Haynes, Cahill, & Narayan, 2018; Bounova & de Weck, 2012; Jamakovic & Uhlig, 2008). A growing body of research suggests that similar patterns of collinearity are observed when applying graph-theoretic principles to structural connectomes, but such observations have not tended to be fully appreciated and are often reported as ancillary findings. In a large sample of over 700 FA-weighted connectomes, theoretically-distinct metrics (Strength, Global Efficiency, and Clustering Coefficient) reported high intercorrelations with one another (all *r*'s > 0.8; Alloza et al., 2018). Such substantial associations have been corroborated in smaller samples but with larger sets of network metrics (Roine et al., 2019). The high degree of overlap between graph-theoretic metrics is also apparent in the functional connectivity literature (Lynall et al., 2010; Li, Wang, De Haan, Stam, & Van Mieghem, 2011). Importantly, some metrics are mathematically dependent, for instance by virtue of being directly proportional to one another (e.g., mean edge weight and Strength; Degree and Density) or conceptual inverses of one another (e.g., Characteristic Path Length and Global Efficiency). Likewise, some metrics may be similar to one another (e.g., efficiency-based measures) because of how they capture local diffusion properties (Goñi et al., 2013). Treating such metrics as conveying separable information is of course problematic. As would be expected, the observed pairwise correlations between these metrics are high, and mean correlations across the full set of metrics may be upwardly biased by the inclusion of mathematically overlapping metrics. Importantly, however, these cases are insufficient to explain the pervasive pattern of interrelatedness documented here, which encompasses both theoretically- and mathematically-distinct metrics (e.g., Clustering Coefficient and Global Efficiency) as well as a metric of connectivity not rooted in graph theory (mean edge weight).

By itself, the substantial collinearity observed between mathematically-distinct network metrics is not necessarily problematic, when such correlations are themselves empirical observations that warrant scientific investigation and explanation. However, the fact that such correlations also arise pervasively across simulation conditions, including conditions in which edges are generated to be essentially uncorrelated, suggest that they may be a byproduct of the analytic approach rather than a meaningful empirical observation. It is also of particular note that graph-theoretic metrics correlated strongly with mean edge weight, a topologically-naïve average of network weights, across virtually all observed and simulated conditions. Of course, the level of collinearity that a researcher finds concerning is at least partly subjective, and may differ depending on the intended application and inferences to be drawn.

From a practical standpoint, researchers planning to use global graph-theoretic metrics to probe more specialized properties of the brain would benefit from examining associations between selected metrics and general summary indices of brain structure before drawing conclusions about the relevance of that specialized property to the outcome under consideration. Our findings converge with recent research in a small clinical sample finding that network properties “provide only a small added benefit” relative to general white matter diffusion metrics and cautioning that metrics such as global efficiency “should thus not be understood as the “efficiency” of the brain network, but rather be interpreted as a global diffusion marker of the brain network.” (Dewenter et al., 2022, pp. 1020; 1030). We extend these findings in a large-scale sample of the general population to show that this pattern extends to multiple metrics beyond global efficiency.

It is well-established that network construction parameters, such as network size and density, can influence the comparison of graph-based metrics (van Wijk, Stam, & Daffertshofer, 2010). Our findings extend this by demonstrating that removing potentially spurious edges or employing measurement schemes that impose greater variation in edge weights may help to reduce correlations among graph-based metrics when applied to structural connectivity data. Thresholding networks at the sample (rather than individual) level is considered advantageous for preserving a common density across individuals, as density is a well-known factor that drives the values of global, mesoscale, and local scale network metrics (van Wijk, Stam, & Daffertshofer, 2010). However, the utility of this strategy will depend both on parameters in the analytical pipeline and on the graph-theoretic metrics under consideration. Degree, Betweenness, Participation Coefficient, and Modularity demonstrated some of the most distinct patterns of interindividual variation, particularly in sparse small-world networks with uncorrelated edges. Likewise, although we examine collinearity amongst metrics across a wide range of network construction parameters, we nevertheless capture only a subset of the array of potential analytic pipelines for processing diffusion MRI data and constructing structural brain networks (Parker et al., 2014). Researchers employing other analytic pipelines would benefit from inspecting the associations amongst relevant graph-theoretic metrics prior to the application of these metrics in primary analyses. For example, although we examine correlations amongst metrics across two commonly-used thresholding schemes, there are alternative schemes for thresholding and streamline reconstruction (e.g., Smith, Tournier, Calamante, & Connelly, 2015) to which the generalizability of our findings is not known.

From a theoretical standpoint, our findings suggest caution in drawing strong conclusions about mechanisms based on associations within individual global graph-theoretic metrics alone. Indeed, a growing theoretical literature has begun to provide a framework for drawing mechanistic explanations from neural networks (Bertolero & Bassett, 2020; Zednik, 2019). Population-level differences in global graph-theoretic metrics derived from static structural brain networks may not be equipped to provide mechanistic insights, even if discriminable, because they fail to capture the dynamic and generative processes through which white matter gives rise to higher-order thought (Bassett, Zurn, & Gold, 2018). Nevertheless, population-level differences in global metrics derived from static structural brain networks can provide useful descriptions of brain organization, architecture and topology, and this “description [can] offer evidence for a mechanistic model.” (Bertolero & Bassett, 2020). Building mechanistic models requires accurate and meaningful descriptions of a system.

Although this study examined a set of commonly-used graph-theoretic metrics in the largest sample of structural connectomes to date, it is not without limitations. First, network science returns an extensive set of graph-theoretic metrics (Bullmore & Sporns, 2009). We selected metrics that are (a) widely-used in the field (Welton, Kent, Auer, & Dineen, 2015; Tsai, 2018; Messaritaki, Dimitriadis, & Jones, 2019; Yuan et al., 2019) and (b) indicative of the major categories of topological organization in a system (e.g., integration, segregation, centrality) (Rubinov & Sporns, 2010). Certainly, researchers have continued to develop novel and sophisticated network metrics since the introduction of the global metrics selected for the current analyses. Nevertheless, we focus on these global metrics as they represent a popular and commonly used application of network neuroscience (Xiong et al., 2022; Samantaray, Saini, & Gupta, 2022; Li et al., 2022; Cai et al., 2022; Prasad et al., 2022), and our general recommendations to examine incremental validity relative to topologically-naïve metrics still pertains to other measures not examined here. Second, our primary analyses were conducted using FA-weighted networks acquired on a single scanner. Network properties are known to be both highly scanner-specific (even if connectome methods are closely matched; Buchanan et al., 2021) and influenced by connectome methods, such as brain parcellation, dMRI processing, and tractography algorithm (Qi et al., 2015). Therefore, findings may differ with other structural connectome data. Further investigation of the discriminant and explanatory validity of graph-based metrics in other types of MRI data (e.g., functional) will be critical for continuing to assess the conditions in which these metrics may inform mechanistic theories about the neural basis of human traits. Relatedly, it is not known whether our data possessed cryptic structure due to either site-specific scanner differences or familial relatedness. Certainly, the UKB imaging protocol was designed to “maximize data compatibility” by having “identical scanners with fixed platforms (i.e., no major software or hardware updates throughout the study)” (Miller et al., 2016, *online methods*) and researchers are currently seeking to elucidate the pervasiveness of family structure on this dataset (Bycroft et al., 2018). Third, our examination of structural brain networks was restricted to metrics that aggregate information across the topology of the whole brain (i.e., global or averaged node-level metrics), collected at a single point in time (Betzel & Bassett, 2017a). Our analyses can only comment on the use of global metrics to compare graph-level differences between people, and it may be that “graph theory... [remains] very beneficial...for pinpointing (local) network features.” (van Wijk, Stam, & Daffertshofer, 2010, pp. 11). Further, network models that represent the human brain across multiple scales of space, time, and topology may help to shift the field’s “current emphasis beyond network taxonomy – i.e., studying subtle individual- or population-level differences in summary statistics – towards a science of mechanisms and processes.” (Betzel & Bassett, 2017b, pp. 2). Lastly, our analyses focused on *individual differences* in global graph metrics, and therefore cannot comment on the utility of absolute mean levels of these metrics for investigating species-typical organizational properties of the human brain. Though there is a high degree of overlap brain structure across individuals (Huntenburg, Bazin, & Margulies, 2018), observed and simulated connectomes in our analyses were not identically structured (e.g., variation in edge weights, presence/absence of edges, degree of small worldness). We agree that “individual differences in network organization [are] an important prerequisite for understanding neural substrates shaping behavior...” (Jo, Faskowitz, Esfahlani, Sporns, & Betzel., 2021, pp. 1). However, the results of the current study suggest that global graph metrics may be limited in their capabilities to provide specific information about these individual differences.

4.1 Conclusions

Network neuroscience is a heterogeneous constellation of methods and analytic techniques for probing the topological organization of the brain. Determining which features of this rapidly expanding toolbox are best equipped for building mechanistic models of the brain is a crucial step in maximizing the return of this field. This study represents a comprehensive investigation into the discriminant and explanatory validity of global graph-based metrics in structural brain networks. Our findings suggest that careful examination of the types of metrics being used and the properties of the network upon which these metrics are based (e.g. network type, sparsity, (co)variation in edge weights) will be critical for gleaning the types of specific and meaningful conclusions that network neuroscience promises to provide.

Acknowledgments

This work was supported by the National Institutes of Health (Grant No. R01AG054628 [to EMT-D]). EMTD is a Faculty Research Associate of the Population Research Center at the University of Texas at Austin, which is supported by NIH grant P2CHD042849. EMTD is a member of the Center on Aging and Population Sciences (CAPS) at The University of Texas at Austin, which is supported by NIH grant P30AG066614. This research was conducted using the UK Biobank Resource (Application No. 10279).

We thank the UK Biobank participants and UK Biobank team for their work in collecting, processing, and disseminating these data for analysis.

Declaration of Competing Interest

IJD is a participant in UK Biobank. All other authors report no biomedical financial interests or potential conflicts of interest.

Data and Code Availability

Raw data from UK Biobank are open to qualified scientists by completing an application here: https://www.ukbiobank.ac.uk/enable-your-research/apply-for-access. Given the computationally-intensive nature of our preprocessing pipeline, derived data supporting the findings of this study and *R* scripts for conducting analyses may be available from corresponding author JWM on request.

References

Alfaro-Almagro, F., Jenkinson, M., Bangerter, N. K., Andersson, J. L. R., Griffanti, L., Douaud, G., … & Smith, S. M. (2018). Image processing and Quality Control for the first 10,000 brain imaging datasets from UK Biobank. *NeuroImage*, *166*, 400–424. https://doi.org/10.1016/j.neuroimage.2017.10.034

Alloza, C., Cox, S. R., Cábez, M. B., Redmond, P., Whalley, H. C., Ritchie, S. J., ... & Wardlaw, J. M. (2018). Polygenic risk score for schizophrenia and structural brain connectivity in older age: A longitudinal connectome and tractography study. *NeuroImage*, *183*, 884-896.

Andreotti, J., Jann, K., Melie-Garcia, L., Giezendanner, S., Dierks, T., & Federspiel, A. (2014). Repeatability analysis of global and local metrics of brain structural networks. *Brain Connectivity*, *4*, 203-220.

Bassett, D. S., & Lynall, M. E. (2013). Network methods to characterize brain structure and function. *Cognitive Neurosciences: The Biology of the Mind*, 1-27.

Bassett, D. S., & Sporns, O. (2017). Network neuroscience. *Nature Neuroscience*, *20*, 353-364.

Bassett, D. S., Zurn, P., & Gold, J. I. (2018). On the nature and use of models in network neuroscience. *Nature Reviews Neuroscience*, *19*, 566-578.

Baum, G. L., Ciric, R., Roalf, D. R., Betzel, R. F., Moore, T. M., Shinohara, R. T., ... & Cook, P. A. (2017). Modular segregation of structural brain networks supports the development of executive function in youth. *Current Biology*, *27*, 1561-1572.

Behrens, T. E., Johansen-Berg, H., Woolrich, M. W., Smith, S. M., Wheeler-Kingshott, C. A. M., Boulby, P. A., ... & Matthews, P. M. (2003). Non-invasive mapping of connections between human thalamus and cortex using diffusion imaging. *Nature Neuroscience*, *6*, 750-757.

Berlot, R., Metzler-Baddeley, C., Ikram, M. A., Jones, D. K., & O'Sullivan, M. J. (2016). Global efficiency of structural networks mediates cognitive control in mild cognitive impairment. *Frontiers in Aging Neuroscience*, *8*, 292.

Bertolero, M. A., & Bassett, D. S. (2020). On the nature of explanations offered by network science: A perspective from and for practicing neuroscientists. *Topics in Cognitive Science*, *12*, 1272-1293.

Betzel, R. F., & Bassett, D. S. (2017a). Multi-scale brain networks. *NeuroImage*, *160*, 73-83.

Betzel, R. F., & Bassett, D. S. (2017b). Generative models for network neuroscience: Prospects and promise. *Journal of The Royal Society Interface*, *14*, 20170623.

Bounova, G., & De Weck, O. (2012). Overview of metrics and their correlation patterns for multiple-metric topology analysis on heterogeneous graph ensembles. *Physical Review E*, *85*, 016117.

Buchanan, C. R., Bastin, M. E., Ritchie, S. J., Liewald, D. C., Madole, J. W., Tucker-Drob, E. M., Deary, I. J., & Cox, S. R. (2020). The effect of network thresholding and weighting on structural brain networks in the UK Biobank. *NeuroImage*, *211*, 116443. https://doi.org/10.1016/j.neuroimage.2019.116443

Buchanan, C. R., Muñoz Maniega, S., Valdés Hernández, M. C., Ballerini, L., Barclay, G., Taylor, A. M., ... & Cox, S. R. (2021). Comparison of structural MRI brain measures between 1.5 and 3 T: Data from the Lothian Birth Cohort 1936. *Human Brain Mapping*, *42*, 3905-3921.

Buchanan, C. R., Pernet, C. R., Gorgolewski, K. J., Storkey, A. J., & Bastin, M. E. (2014). Test–retest reliability of structural brain networks from diffusion MRI. *NeuroImage*, *86*, 231–243. https://doi.org/10.1016/j.neuroimage.2013.09.054

Buchanan, C. R., Pettit, L. D., Storkey, A. J., Abrahams, S., & Bastin, M. E. (2015). Reduced structural connectivity within a prefrontal-motor-subcortical network in amyotrophic lateral sclerosis. *Journal of Magnetic Resonance Imaging: JMRI*, *41*, 1342–1352. https://doi.org/10.1002/jmri.24695

Bullmore, E., & Sporns, O. (2009). Complex brain networks: graph theoretical analysis of structural and functional systems. *Nature Reviews Neuroscience*, *10*, 186-198.

Bycroft, C., Freeman, C., Petkova, D., Band, G., Elliott, L. T., Sharp, K., … & Marchini, J. (2018). The UK Biobank resource with deep phenotyping and genomic data. *Nature, 562*, 203-209.

Cai, M., Jacob, M.A., Norris, D. G., De Leeuw, F. E., & Tuladhar, A. M. (2022). Longitudinal relation between structural network efficiency, cognition, and gait in cerebral small vessel disease. *The Journals of Gerontology: Series A*, *77*, 554-560.

Candeloro, L., Savini, L., & Conte, A. (2016). A new weighted degree centrality measure: The application in an animal disease epidemic. *PloS One*, *11*, e0165781.

Christensen, A.P. (2018). “NetworkToolbox: Methods and measures for brain, cognitive, and psychometric network analysis in R.” *The R Journal*, 422–439. https://doi.org/10.32614/RJ-2018-065.

Cohen, J. (1988). Statistical Power Analysis for the Behavioral Sciences (2nd ed.). Hillsdale, NJ: Lawrence Erlbaum Associates, Publishers.

Cox, S. R., & Deary, I. J. (2022). Brain and cognitive ageing: The present, and some predictions (… about the future). *Aging Brain*, *2*, 100032.

Cox, S.R., Ritchie, S. J., Fawns-Ritchie, C., Tucker-Drob, E. M., & Deary, I. J. (2019). Structural brain imaging correlates of general intelligence in UK Biobank. *Intelligence*, *76*, 101376. https://doi.org/10.1016/j.intell.2019.101376

Csardi, G., & Nepusz, T. (2006). The igraph software package for complex network research. *InterJournal, Complex Systems*, *1695*, 1-9.

Darst, R.K., Reichman, D.R., Ronhovde, P., & Nussinov, Z. (2013). An edge density definition of overlapping and weighted graph communities. *arXiv preprint arXiv:1301.3120*.

Deary, I. J., Cox, S. R., & Hill, W. D. (2021). Genetic variation, brain, and intelligence differences. *Molecular Psychiatry*, 1-19.

Deary, I. J., Ritchie, S. J., Muñoz Maniega, S., Cox, S. R., Valdés Hernández, M. C., Luciano, M., ... & Bastin, M. E. (2019). Brain peak width of skeletonized mean diffusivity (PSMD) and cognitive function in later life. *Frontiers in Psychiatry*, 524.

Desikan, R. S., Ségonne, F., Fischl, B., Quinn, B. T., Dickerson, B. C., Blacker, D., Buckner, R. L., Dale, A. M., Maguire, R. P., Hyman, B. T., Albert, M. S., & Killiany, R. J. (2006). An automated labeling system for subdividing the human cerebral cortex on MRI scans into gyral based regions of interest. *NeuroImage*, *31*, 968–980. https://doi.org/10.1016/j.neuroimage.2006.01.021

Dewenter, A., Gesierich, B., Ter Telgte, A., Wiegertjes, K., Cai, M., Jacob, M. A., ... & Duering, M. (2022). Systematic validation of structural brain networks in cerebral small vessel disease. *Journal of Cerebral Blood Flow & Metabolism*, *42*, 1020-1032.

Farahani, F. V., Karwowski, W., & Lighthall, N. R. (2019). Application of graph theory for identifying connectivity patterns in human brain networks: a systematic review. *Frontiers in Neuroscience*, *13*, 585. https://doi.org/10.3389/fnins.2019.00585

Fischl, B., & Dale, A. M. (2000). Measuring the thickness of the human cerebral cortex from magnetic resonance images. *Proceedings of the National Academy of Sciences*, *97*, 11050-11055.

Fischl, B. (2012). FreeSurfer. *Neuroimage*, *62*, 774-781.

Girvan, M., & Newman, M. E. (2002). Community structure in social and biological networks. *Proceedings of the National Academy of Sciences*, *99*, 7821-7826.

Gignac, G. E., & Bates, T. C. (2017). Brain volume and intelligence: The moderating role of intelligence measurement quality. *Intelligence*, *64*, 18–29. https://doi.org/10.1016/j.intell.2017.06.004

Glasser, M.F., Coalson, T.S., Robinson, E.C., Hacker, C.D., Harwell, J., Yacoub, E., … & Van Essen, D.C. (2016). A multi-modal parcellation of human cerebral cortex. *Nature*, *536*, 171-178.

Godwin, D., Barry, R. L., & Marois, R. (2015). Breakdown of the brain's functional network modularity with awareness. *Proceedings of the National Academy of Sciences*, *112*, 3799-3804.

Goñi, J., Avena-Koenigsberger, A., Velez de Mendizabal, N., van den Heuvel, M. P., Betzel, R. F., & Sporns, O. (2013). Exploring the morphospace of communication efficiency in complex networks. *PLoS One*, *8*, e58070.

Hagmann, P., Sporns, O., Madan, N., Cammoun, L., Pienaar, R., Wedeen, V. J., ... & Grant, P. E. (2010). White matter maturation reshapes structural connectivity in the late developing human brain. *Proceedings of the National Academy of Sciences*, *107*, 19067-19072.

Haneef, Z., Levin, H. S., & Chiang, S. (2015). Brain graph topology changes associated with anti-epileptic drug use. *Brain Connectivity*, *5*, 284-291.

Huntenburg, J. M., Bazin, P. L., & Margulies, D. S. (2018). Large-scale gradients in human cortical organization. *Trends in Cognitive Sciences*, *22*, 21-31.

Jamakovic, A., & Uhlig, S. (2008). On the relationships between topological measures in real-world networks. *NHM*, *3*, 345-359.

Jo, Y., Faskowitz, J., Esfahlani, F. Z., Sporns, O., & Betzel, R. F. (2021). Subject identification using edge-centric functional connectivity. *NeuroImage*, *238*, 118204.

Joyce, K. E., Laurienti, P. J., Burdette, J. H., & Hayasaka, S. (2010). A new measure of centrality for brain networks. *PloS One*, *5*, e12200.

Kenny, D. A. (2015). Measuring model fit.

Kim, D. J., Davis, E. P., Sandman, C. A., Sporns, O., O'Donnell, B. F., Buss, C., & Hetrick, W. P. (2016). Children's intellectual ability is associated with structural network integrity. *NeuroImage*, *124*, 550-556.

Kogotkova, S., Oehlers, M., Ermakova, T., & Fabian, B. (2018). Correlation Analysis of Local Graph Metrics. *Available at SSRN 3192028*.

Li, C., Wang, H., De Haan, W., Stam, C. J., & Van Mieghem, P. (2011). The correlation of metrics in complex networks with applications in functional brain networks. *Journal of Statistical Mechanics: Theory and Experiment*, *2011*, P11018.

Li, W., Wang, L., Lyu, Z., Chen, J., Li, Y., Sun, Y.,… & Li, Q. (2022). Difference in topological organization of white matter structural connectome between methamphetamine and heroin use disorder. *Behavioural Brain Research*, *422*, 113752.

Li, Y., Liu, Y., Li, J., Qin, W., Li, K., Yu, C., & Jiang, T. (2009). Brain anatomical network and intelligence. *PLoS Computational Biology*, *5*, e1000395.

Lynall, M. E., Bassett, D. S., Kerwin, R., McKenna, P. J., Kitzbichler, M., Muller, U., & Bullmore, E. (2010). Functional connectivity and brain networks in schizophrenia. *Journal of Neuroscience*, *30*, 9477-9487.

Madole, J. W., Ritchie, S. J., Cox, S. R., Buchanan, C. R., Hernández, M. V., Maniega, S. M., ... & Tucker-Drob, E. M. (2021). Aging-sensitive networks within the human structural connectome are implicated in late-life cognitive declines. *Biological Psychiatry*, *89*, 795-806.

Marek, S., Tervo-Clemmens, B., Calabro, F. J., Montez, D. F., Kay, B. P., Hatoum, A. S., ... & Dosenbach, N. U. (2022). Reproducible brain-wide association studies require thousands of individuals. *Nature*, 1-7.

Messaritaki, E., Dimitriadis, S. I., & Jones, D. K. (2019). Optimization of graph construction can significantly increase the power of structural brain network studies. *NeuroImage*, *199*, 495-511.

Miller, K. L., Alfaro-Almagro, F., Bangerter, N. K., Thomas, D. L., Yacoub, E., Xu, J., … & Smith, S. M. (2016). Multimodal population brain imaging in the UK Biobank prospective epidemiological study. *Nature Neuroscience*, *19*, 1523–1536. https://doi.org/10.1038/nn.4393

Nave, G., Jung, W. H., Karlsson Linnér, R., Kable, J. W., & Koellinger, P. D. (2019). Are bigger brains smarter? Evidence from a large-scale preregistered study. *Psychological Science*, *30*, 43-54.

Parker, C. S., Deligianni, F., Cardoso, M. J., Daga, P., Modat, M., Dayan, M., ... & Clayden, J. D. (2014). Consensus between pipelines in structural brain networks. *Plos One*, *9*, e111262.

Pereira, J. B., Aarsland, D., Ginestet, C. E., Lebedev, A. V., Wahlund, L. O., Simmons, A., ... & Westman, E. (2015). Aberrant cerebral network topology and mild cognitive impairment in early Parkinson's disease. *Human Brain Mapping*, *36*, 2980-2995.

Pietschnig, J., Penke, L., Wicherts, J. M., Zeiler, M., & Voracek, M. (2015). Meta-analysis of associations between human brain volume and intelligence differences: How strong are they and what do they mean? *Neuroscience & Biobehavioral Reviews*, *57*, 411–432. https://doi.org/10.1016/j.neubiorev.2015.09.017

Prasad, K., Rubin, J., Mitra, A., Lewis, M., Theis, N., Muldoon, B., … & Cape, J. (2022). Structural covariance networks in schizophrenia: A systematic review part II. *Schizophrenia Research*, *239*, 176-191.

Qi, S., Meesters, S., Nicolay, K., ter Haar Romeny, B. M., & Ossenblok, P. (2015). The influence of construction methodology on structural brain network measures: A review. *Journal of Neuroscience Methods*, *253*, 170-182.

Roberts, J. A., Perry, A., Roberts, G., Mitchell, P. B., & Breakspear, M. (2017). Consistency-based thresholding of the human connectome. *NeuroImage*, *145*, 118–129. https://doi.org/10.1016/j.neuroimage.2016.09.053

Robinson, E.C., Hammers, A., Ericsson, A., Edwards, A.D., Rueckert, D. (2010). Identifying population differences in whole-brain structural networks: A machine learning approach. *NeuroImage, 50*, 910–919. https://doi.org/10.1016/ j.neuroimage.2010.01.019.

Roine, T., Jeurissen, B., Perrone, D., Aelterman, J., Philips, W., Sijbers, J., & Leemans, A. (2019). Reproducibility and intercorrelation of graph theoretical measures in structural brain connectivity networks. *Medical Image Analysis*, *52*, 56-67.

Rubinov, M., Sporns, O., van Leeuwen, C., & Breakspear, M. (2009). Symbiotic relationship between brain structure and dynamics. *BMC Neuroscience*, *10*, 1-18.

Rubinov, M., & Sporns, O. (2010). Complex network measures of brain connectivity: uses and interpretations. *NeuroImage*, *52*, 1059-1069.

Samantaray, T., Saini, J., & Gupta, C. N. (2022, July). Sparsity dependent metrics depict alteration of brain network connectivity in Parkinson's disease. In *2022 44th Annual*

International Conference of the IEEE Engineering in Medicine & Biology Society (EMBC) (pp. 698-701). IEEE.

Smith, R. E., Tournier, J. D., Calamante, F., & Connelly, A. (2015). SIFT2: Enabling dense quantitative assessment of brain white matter connectivity using streamlines tractography. *NeuroImage*, *119*, 338-351.

Sporns, O. (2013). Structure and function of complex brain networks. *Dialogues in Clinical Neuroscience*, *15*, 247–262. https://doi.org/10.31887/DCNS.2013.15.3/osporns

Strang, A., Haynes, O., Cahill, N. D., & Narayan, D. A. (2018). Generalized relationships between characteristic path length, efficiency, clustering coefficients, and density. *Social Network Analysis and Mining*, *8*, 1-6.

Sudlow, C., Gallacher, J., Allen, N., Beral, V., Burton, P., Danesh, J., ... & Collins, R. (2015). UK Biobank: An open access resource for identifying the causes of a wide range of complex diseases of middle and old age. *PLoS Medicine*, *12*, e1001779. https://doi.org/10.1371/journal.pmed.1001779

Tompson, S. H., Falk, E. B., Vettel, J. M., & Bassett, D. S. (2018). Network approaches to understand individual differences in brain connectivity: Opportunities for personality neuroscience. *Personality Neuroscience*, *1*. https://doi.org/10.1017/pen.2018.4

Tsai, S. Y. (2018). Reproducibility of structural brain connectivity and network metrics using probabilistic diffusion tractography. *Scientific Reports*, *8*, 1-12.

Van Montfort, S. J. T., van Dellen, E., Stam, C. J., Ahmad, A. H., Mentink, L. J., Kraan, C. W., ... & Slooter, A. J. C. (2019). Brain network disintegration as a final common pathway for delirium: A systematic review and qualitative meta-analysis. *NeuroImage: Clinical*, *23*, 101809.

Van Wijk, B. C., Stam, C. J., & Daffertshofer, A. (2010). Comparing brain networks of different size and connectivity density using graph theory. *PloS One*, *5*, e13701.

Váša, F., & Mišić, B. (2022). Null models in network neuroscience. *Nature Reviews Neuroscience*, 1-12.

Verstraete, E., Veldink, J.H., Mandl, R.C.W., Van Den Berg, L.H., Van Den Heuvel, M.P. (2011). Impaired structural motor connectome in amyotrophic lateral sclerosis. *PLoS One*, *6,* e24239. https://doi.org/10.1371/journal.pone.0024239.

Wang, J., Zuo, X., & He, Y. (2010). Graph-based network analysis of resting-state functional MRI. *Frontiers in Systems Neuroscience*, *4*, 16.

Watson, C.G. (2020). brainGraph: Graph theory analysis of brain MRI data. R package version 3.0.0. https://CRAN.R-project.org/package=brainGraph

Welton, T., Kent, D.A., Auer, D.P., & Dineen, R.A. (2015). Reproducibility of graph-theoretic brain network metrics: A systematic review. *Brain Connectivity*, *5*, 193-202.

Xiong, Y., Tian, T., Fan, Y., Yang, S., Xiong, X., Zhang, Q., & Zhu, W. (2022). Diffusion tensor imaging reveals altered topological efficiency of structural networks in type-2 diabetes patients with and without mild cognitive impairment. *Journal of Magnetic Resonance Imaging*, *55*, 917-927.

Yao, Z., Zou, Y., Zheng, W., Zhang, Z., Li, Y., Yu, Y., ... & Hu, B. (2019). Structural alterations of the brain preceded functional alterations in major depressive disorder patients: Evidence from multimodal connectivity. *Journal of Affective Disorders*, *253*, 107-117.

Yuan, J. P., Henje Blom, E., Flynn, T., Chen, Y., Ho, T. C., Connolly, C. G., … & Tymofiyeva, O. (2019). Test-retest reliability of graph theoretic metrics in adolescent brains. *Brain Connectivity*, *9*, 144-154.

Zednik, C. (2019). Models and mechanisms in network neuroscience. *Philosophical Psychology*, *32*, 23-51.

Zhang, H., Schneider, T., Wheeler-Kingshott, C. A., & Alexander, D. C. (2012). NODDI: practical in vivo neurite orientation dispersion and density imaging of the human brain. *NeuroImage*, *61*, 1000-1016.

Zhou, C., Ping, L., Chen, W., He, M., Xu, J., Shen, Z., ... & Cheng, Y. (2021). Altered white matter structural networks in drug-naive patients with obsessive-compulsive disorder. *Brain Imaging and Behavior*, *15*, 700-710.

Supplementary Materials

Table S1. **Average absolute correlations between network metrics in unthresholded FA-weighted networks.**

Metric	**Mean |*r*| with other metrics**	**Range of |*r's*| with other metrics**
Participation Coefficient	0.099	0.034 - 0.314
Metric	**Mean |*r*| with other metrics (excluding Participation Coefficient)**	**Range of |*r's*| with other metrics (excluding Participation Coefficient)**
Density	0.740	0.561 - 1.00
Degree	0.740	0.561 - 1.00
Strength	0.873	0.693 - 0.938
Betweenness	0.732	0.549 - 0.996
Closeness	0.797	0.476 - 0.996
Characteristic Path Length	0.799	0.481 - 0.996
Global Efficiency	0.776	0.445 - 0.993
Clustering Coefficient	0.788	0.508 - 0.990
Modularity	0.621	0.445 - 0.833
Small Worldness	0.802	0.496 - 0.994

Note. Due to the dissociability of Participation Coefficient from all other metrics, this metric was excluded from estimates of average absolute correlations to improve detection of dissociability amongst other network metrics.

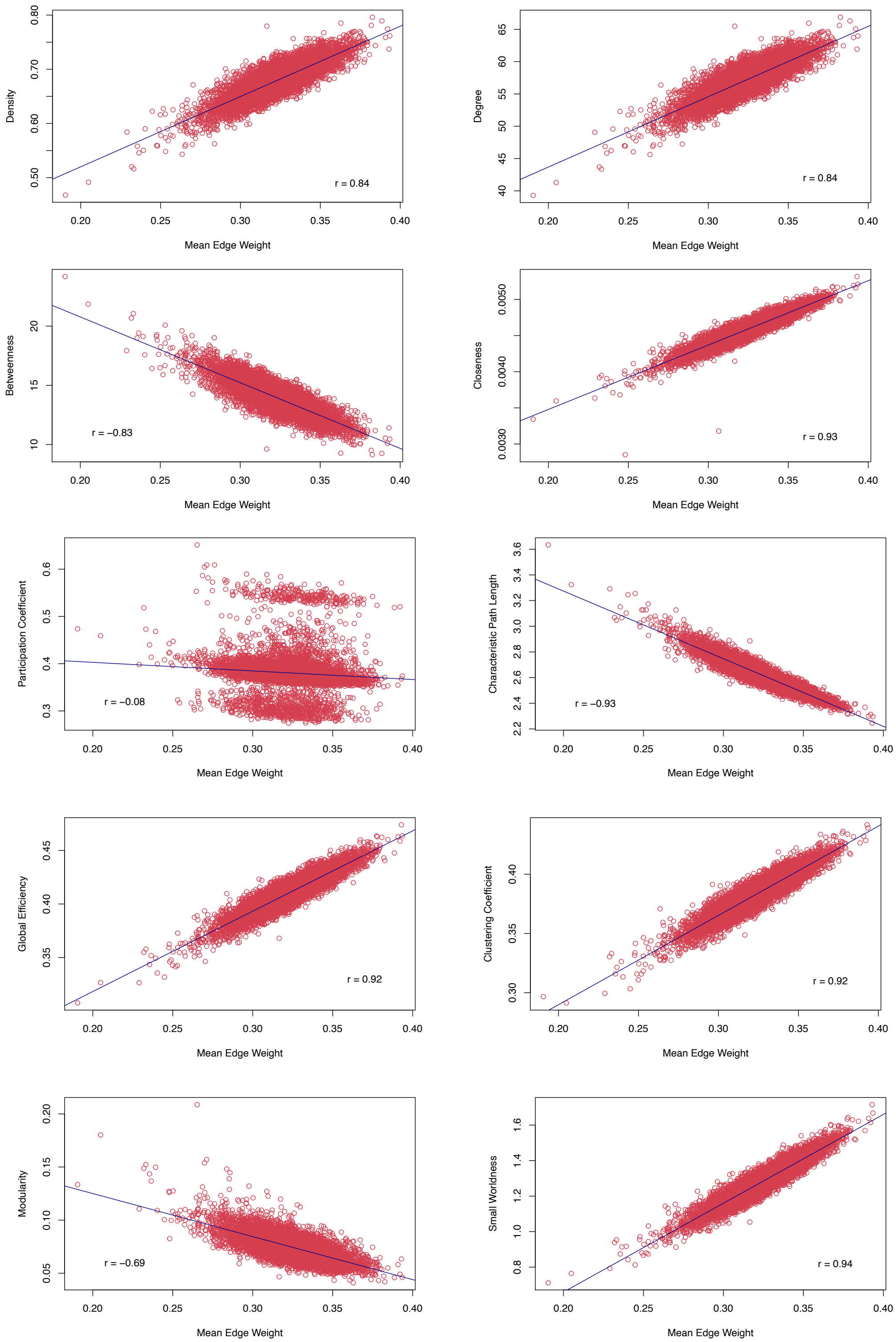

Figure S1. Scatterplots of associations between mean edge weight and each graph-theoretic metric in unthresholded, FA-weighted networks. Association between mean edge weight and Strength is not displayed due to perfect collinearity between these two estimates.

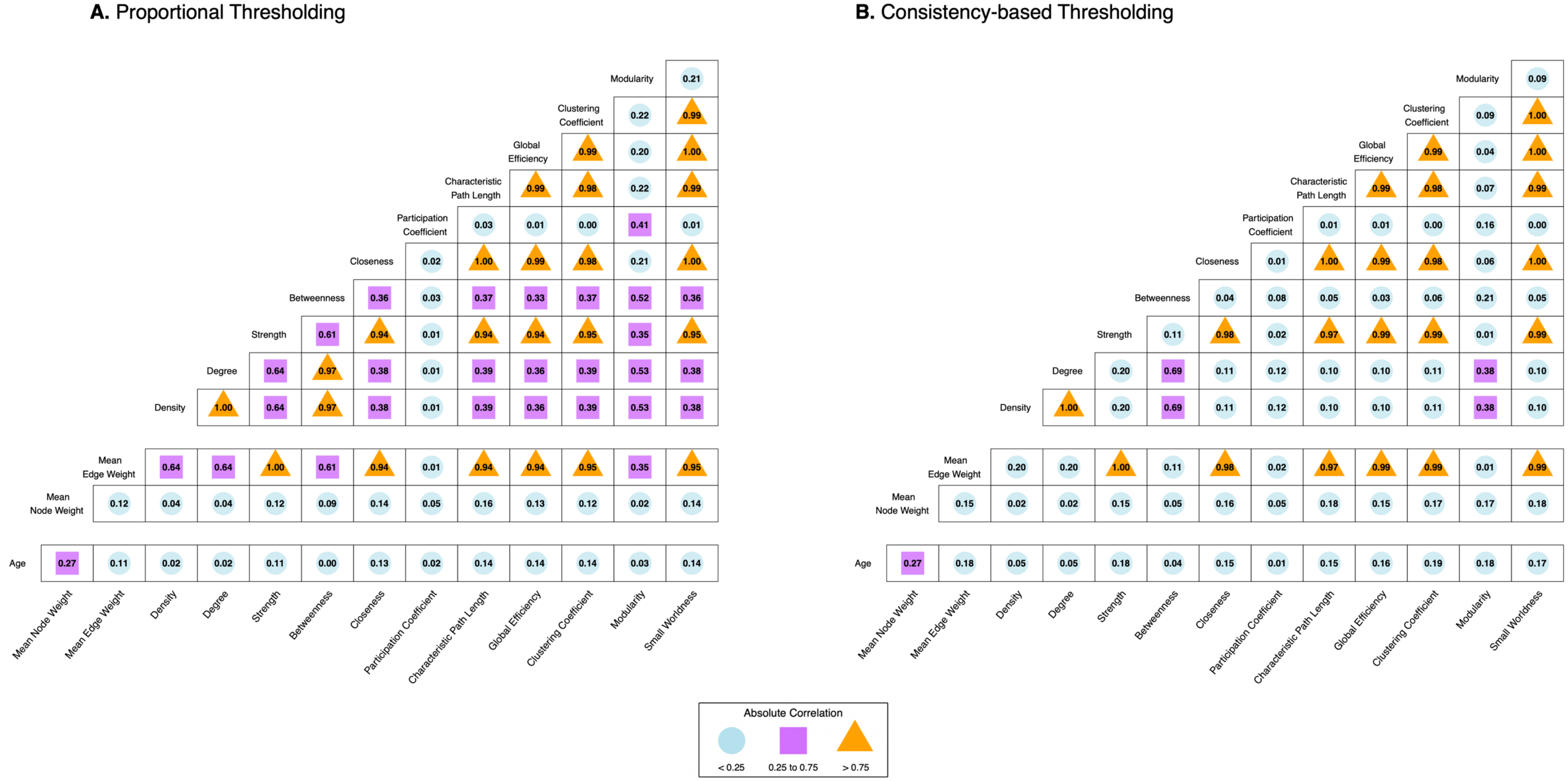

Figure S2. Correlations between A) proportional thresholded FA-weighted network metrics, mean edge and node weight, and age and B) consistency-based thresholded FA-weighted network metrics, mean edge and node weight, and age. Cells display absolute correlations for sake of interpretation.

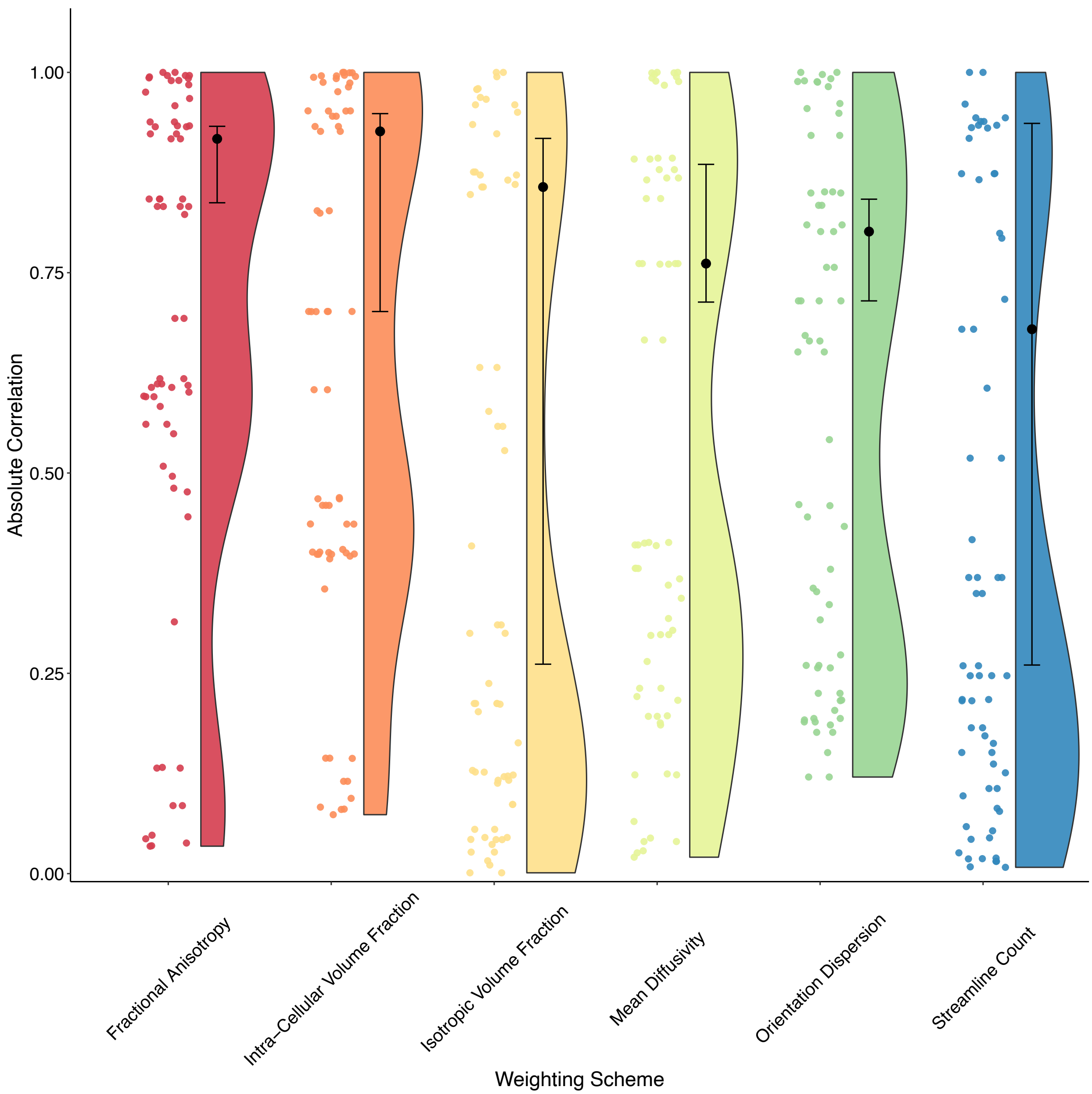

Figure S3. Raincloud plots reflecting distributions of absolute correlations between network metrics estimated for each dMRI weighting scheme. Density distributions reflect absolute correlations amongst each of the 11 network metrics, excluding mean edge weight. Individual data points reflect pairwise absolute associations between network metrics. Overlaid boxplot reflects interquartile range of distribution of absolute correlations between each network metric and mean edge weight. Code for this plot was adapted from https://gist.github.com/dgrtwo/eb7750e74997891d7c20 and https://wellcomeopenresearch.org/articles/4-63/v1.